

D²F2WOD: Learning Object Proposals for Weakly-Supervised Object Detection via Progressive Domain Adaptation

Yuting Wang
Rutgers University
Piscataway, NJ

yw632@cs.rutgers.edu

Ricardo Guerrero
Samsung AI Center
Cambridge, UK

r.guerrero@samsung.com

Vladimir Pavlovic
Rutgers University
Piscataway, NJ

vladimir@cs.rutgers.edu

Abstract

Weakly-supervised object detection (WSOD) models attempt to leverage image-level annotations in lieu of accurate but costly-to-obtain object localization labels. This oftentimes leads to substandard object detection and localization at inference time. To tackle this issue, we propose D²F2WOD, a **D**ual-**D**omain **F**ully-to-**W**eakly **S**upervised **O**bject **D**etection framework that leverages synthetic data, annotated with precise object localization, to supplement a natural image target domain, where only image-level labels are available. In its warm-up domain adaptation stage, the model learns a fully-supervised object detector (FSOD) to improve the precision of the object proposals in the target domain, and at the same time learns target-domain-specific and detection-aware proposal features. In its main WSOD stage, a WSOD model is specifically tuned to the target domain. The feature extractor and the object proposal generator of the WSOD model are built upon the fine-tuned FSOD model. We test D²F2WOD on five dual-domain image benchmarks. The results show that our method results in consistently improved object detection and localization compared with state-of-the-art methods.

1. Introduction

Object detection has achieved remarkable progress over the past few years, mostly through the development of deep neural network architectures [21, 4]. However, training such deep neural networks needs large amounts of manually annotated images. Obtaining these annotations is costly and time-consuming. Thus, reducing these costs is of great importance, and many weakly-supervised object detection (WSOD) methods [2, 32, 31] have been developed accordingly. WSOD methods alleviate the reliance on precise object localization information by training detection architectures using only *image-level* annotations.

Most existing WSOD algorithms [2, 32, 31, 37, 22, 8, 14]

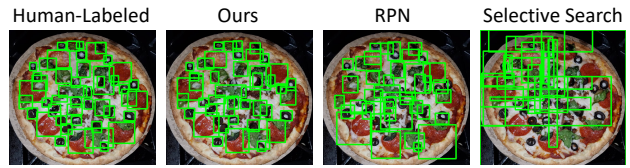


Figure 1: Illustration of human-labeled objects contrasted to object proposals generated by our D²F2WOD_{warm-up}, RPN of Faster R-CNN trained on synthetic data alone, and Selective Search (SS), on the RealPizza10 dataset. It demonstrates the benefit of our learned object proposal generator (warm-up stage) over SS. SS often fails to generate accurate bounding boxes, making it hard to improve classification accuracy. It also shows that our D²F2WOD_{warm-up} is better than learned RPN of Faster R-CNN trained on synthetic data alone. Our warm-up domain adaptation stage can improve the precision of the object proposals in the target domain.

are based on multiple instance learning (MIL) [6]. They treat images as bags of object proposals, which are produced by an object proposal generator [34, 44]. Although many promising results have been achieved by WSOD, they are still not comparable to fully-supervised object detectors (FSOD) [21, 4]. One of the main reasons is that state-of-the-art object proposal generators still cannot produce accurate object proposals – this is a particularly serious issue for *in-the-wild* images with multiple complex non-rigid objects and cluttered background, as shown in Fig. 1.

To overcome this difficulty, we introduce a simple object proposal generation strategy that can be applied to different WSODs to improve their detection performance. Our key insight is to cast WSOD as a *domain adaptation problem* – while target “natural” images often lack localization labels, localization is “freely” available for “non-photographic” synthetic images. For instance, when synthesizing images such as SyntheticPizza10 [20], localization and identity labels are available as a byproduct of the generation process. Highly stylized images (e.g., Clipart1K [15], Watercolor2K [15], and Comic2K [15]) are likewise easier to annotate than natural images, where objects may exhibit com-

plex changes in shape or appearance. In this work, we are interested in leveraging fully-annotated non-photographic datasets to support accurate object localization in real-world datasets. To this end, we propose a **Dual-Domain Fully-to-Weakly Supervised Object Detection** (D^2F2WOD) framework, which is able to produce accurate object proposals using image-level labels of natural images along with fully-supervised non-photographic images through *progressive domain adaptation* of an FSOD model.

Given the large domain gap between the source and the target, across both foreground and background (F&B), it is critical to (1) individually address the adaptation of F&B in a disentangled manner when feasible, and (2) reduce the domain gap in a gradual manner to control the propagation of errors. In our work, we progressively adapt an FSOD model from source images to the target domain in five steps. First, we build an initial bridge between the non-photographic source and the real-world target domains using unpaired image-to-image translation (I2I), such as [43]. This creates “target-like” intermediate images with location-accurate object instances but divergent appearance. Instead of the common practice of initializing an FSOD on this intermediate domain, we further reduce the domain gap by employing a copy-paste augmentation technique sourced in [38, 9] to fuse the translated object appearance with real background images and create a second transfer-labeled intermediate domain. This domain serves as the preliminary stage for initializing an FSOD, to be used for pseudo labeling (PL) [17] in the subsequent WSOD learning phase on the real target domain. However, the typical number of confident pseudo-labeled instances resulting from the initialized FSOD and needed for WSOD is insufficient for effective adaptation to the target domain. To that end, we re-employ the previously used augmentation technique to increase the number of confident PL instances. Finally, we learn a detection head utilizing these target-like object proposal features. Our D^2F2WOD achieves consistent improvements compared with the state-of-the-art methods, offering a strong baseline for WSOD models.

Our contributions are three-fold: (1) We propose a framework for object proposal generation based on domain adaptation, applicable to different WSODs, including OICR [32], and CASD [14]. The five-step progressive domain adaptation process exploits gradual adaptation of the FSOD on generated samples, as well as with decoupled focus on foreground and background, and it can be seamlessly integrated with different types of FSOD backbones such as Faster R-CNN [21] and transformer-based detectors [4]. (2) We construct a dual-domain image benchmark SyntheticPizza10 \rightarrow RealPizza10 with non-photographic images as the source and real-world images as the target domains. (3) The experimental results show that our D^2F2WOD achieves state-of-the-art performance on five benchmarks.

2. Related Work

Weakly-Supervised Object Detection. WSOD methods generally aim to exploit only image-level annotations, as opposed to the fine-grained object localization usually used in FSOD. Existing methods mainly cast WSOD as a multiple-instance learning (MIL) problem, where objects are not necessarily centered in images and there is cluttered background [19]. In MIL-based models, an image is interpreted as a bag of potential object instances. These models generally consist of three components: feature extractor (FE), object proposal (OP) generator, and detection head (DH). Given an image, they first feed it into the OP generator and the FE to generate proposals and feature maps, respectively. Then, the feature maps and object proposals (OPs) are forwarded into a Spatial Pyramid Pooling (SPP) layer [35] or a Region-of-Interest (RoI) pooling layer [21] to produce fixed-size object proposal features. Finally, these feature vectors are fed into the DH to classify and localize objects. End-to-end weakly-supervised deep detection network (WSDNN) [2] proposes one of the first MIL frameworks. Based on Fast R-CNN [10], it introduces a two-stream network to perform classification and localization, respectively. However, in WSDNN, the top ranking OPs may only cover the most discriminative parts of the objects instead of whole object instances, due to a lack of supervision in terms of precise localization information in the training process. Subsequent work [32, 31, 37, 1, 39, 22, 8, 14, 33] aims to alleviate this problem by extending WSDNN. One of the key factors that affect the performance of WSOD is the quality of OPs. Many existing methods are built upon unsupervised RoI extraction, such as selective search (SS) [34] and edge boxes (EB) [44]. To generate OPs, SS uses both exhaustive search and segmentation, and EB uses object edges. [40] proposes a hierarchical region proposal refinement network and [33] proposes a two-stage region proposal network, to refine proposals gradually. Some other work, such as W2N [13], continues refine the noisy dataset generated by a well-trained WSOD with semi-supervised learning.

Different from the above methods, in this work, we first cast WSOD as a domain adaptation problem, by leveraging an auxiliary source domain to pre-train an FSOD model. The FSOD model is progressively adapted from the source to the target domains. After we obtain the adapted FSOD model, we treat it as the weakly-supervised OP generator in the WSOD settings, and at the same time the FE of the FSOD is treated as the pre-trained FE for the WSOD model.

Domain Adaptation for Object Detection. Domain adaptation typically involves two domains, namely source and target domains. Most of existing domain adaptation methods aim to address the domain shift between a fully-labeled source domain and an unlabeled or weakly-labeled target domain, which is formulated as unsupervised or weakly-

supervised domain adaptation, respectively. State-of-the-art domain adaptation for object detection introduces different strategies to reduce the domain divergence. For example, adversarial feature learning is leveraged to adapt object detectors to a target domain with the help of a domain discriminator [5, 27, 29, 12, 36], thus producing domain-invariant features. Highly confident predictions generated by a source detector are used as pseudo-labels to fine-tune the detector on the target domain [15, 16, 42, 25]. Similarly, an unpaired I2I model [15, 23, 12] can be employed to map a source image to a target-like image. Introducing this target-like domain mitigates the difficulty of direct transfer between source and target with a large domain gap.

Different from the aforementioned approaches, our method decouples the domain shift into the foreground and background shift. This makes it possible to gradually, in a focused manner, adapt the detector from source to target. We also use data augmentation in the adaptation stage, since augmentations such as color jittering [30], mixup [41] and copy-paste [38, 9] can have major impact on image classification and object detection. Furthermore, OPs generated by the adapted object detector are augmented by an additional refinement of proposal branches using the detection heads in the WSOD settings. This refinement improves the network’s ability to classify and localize the OPs.

3. Methodology

The proposed Dual-Domain Fully-to-Weakly Supervised Object Detection framework (D²F2WOD) aims to address the lack of object localization information in the target domain by formulating WSOD as a domain adaptation problem. It decouples WSOD model training into two stages – domain adaptation and WSOD. In the domain adaptation stage, we *progressively* learn a domain-adaptive FSOD by leveraging an auxiliary source domain as warm-up. In the WSOD stage, this adapted FSOD is used to initialize the WSOD model, which is then refined on the target domain. D²F2WOD is a general framework that can employ different FSOD and WSOD methods. Here, we focus on two representative FSOD backbones – Faster R-CNN [21] and DETR [4], and two representative WSOD models – the widely-used OICR [32] and the state-of-the-art CASD [14]. In this section, we first formulate the problem, followed by the framework overview, the details of the architecture, and the training procedure for each stage of D²F2WOD.

3.1. Problem Formulation

Fig. 2 illustrates our D²F2WOD approach. Our goal is to detect object instances in a real-world, weakly-supervised target domain \mathcal{T} (e.g., real pizza in Fig. 2) by leveraging a non-photographic source domain \mathcal{S} (e.g., synthetic pizza in Fig. 2). For this problem, we have access to images with only image-level annotations (i.e., class labels) in \mathcal{T} and im-

ages with rich instance-level annotations (i.e., class labels and bounding boxes) in \mathcal{S} .

Formally, $\mathbf{X}_s \in \mathbb{R}^{h \times w \times 3}$ denotes an RGB image from \mathcal{S} , where h and w are the height and width of the image, respectively. $\mathbf{Y}_s^{(f)} = \{(\mathbf{b}_1, c_1), \dots, (\mathbf{b}_{N_s}, c_{N_s})\}$ indicates the instance-level full-annotation associated with \mathbf{X}_s , where $\mathbf{b}_i \in \mathbb{R}^4$ is the i -th object localization bounding box defined by $[x_{\min}, y_{\min}, x_{\max}, y_{\max}]$ that specifies its top-left corner (x_{\min}, y_{\min}) and its bottom-right corner (x_{\max}, y_{\max}) , and $c_i \in \{1, \dots, C\}$ is its category label. N_s is the number of object instances associated with \mathbf{X}_s . The classes to be detected in \mathcal{T} are shared with \mathcal{S} , and C is the number of object categories in the two domains. Similarly, $\mathbf{X}_t \in \mathbb{R}^{h \times w \times 3}$ denotes an RGB image from \mathcal{T} , and $\mathbf{Y}_t^{(w)} = [y_1, \dots, y_C] \in \{0, 1\}^C$ denotes the image-level weak-supervision, where $y_c \in \{0, 1\}$ indicates the absence (presence) of at least one instance of c -th category. N_t is the number of present object classes associated with \mathbf{X}_t . We denote \mathbf{V}_j as object proposal feature vectors of images from domain $j \in \{\mathcal{S}, \mathcal{T}\}$. In this work, we aim to learn an object detector for the target domain, $\hat{\mathbf{Y}}^{(f)} = f(\mathbf{X}|\theta)$, $\mathbf{X} \in \mathcal{T}$, by leveraging both the fully annotated data $\mathcal{D}_s = \{(\mathbf{Y}_s^{(f)}, \mathbf{X}_s)\}$ from \mathcal{S} and the weakly annotated data $\mathcal{D}_t = \{(\mathbf{Y}_t^{(w)}, \mathbf{X}_t)\}$ from \mathcal{T} ; in other words, $\theta^* \leftarrow \mathcal{D} = \{\mathcal{D}_s \cup \mathcal{D}_t\}$.

3.2. Approach Overview

To boost the performance of a WSOD model on \mathcal{T} , our key insight is to jointly improve the precision of the OPs, and learn *target-domain-specific* and *detection-aware* proposal features. To this end, our D²F2WOD exploits the fully-labeled \mathcal{S} (FLS) domain and introduces a dual-stage training scheme as shown in Fig. 2. In the *warm-up* domain adaptation stage, an FSOD is pre-trained (PT) on \mathcal{S} and progressively fine-tuned (FT) on (1) a transfer-labeled intermediate (TLI) domain \mathcal{G}_1 , (2) an augmented (Aug.) transfer-labeled intermediate domain \mathcal{G}_2 , and then on (3) the pseudo-labeled target (PLT) domain \mathcal{T} and (4) the augmented pseudo-labeled target domain \mathcal{T} . As shown in Fig. 2, \mathcal{G}_1 is constructed as target-like instances with accurate transferred localization information, and \mathcal{G}_2 is constructed as target-like images with accurate transferred localization information and real background, thus bridging the \mathcal{S} and \mathcal{T} and facilitating the adaptation. In the *main* WSOD stage, an MIL-based WSOD model is specifically tuned to \mathcal{T} . The FE and the OP generator of the WSOD model are built upon the fine-tuned FSOD model.

3.3. Warm-Up Domain Adaptation Stage: Learning Domain-Specific Features & Object Proposals

The warm-up stage of D²F2WOD trains an FSOD model on the dual \mathcal{S} - \mathcal{T} , which provides the pre-trained deep FE and OP generator to produce object proposal feature vectors on \mathcal{T} . This FSOD model is later used in the main

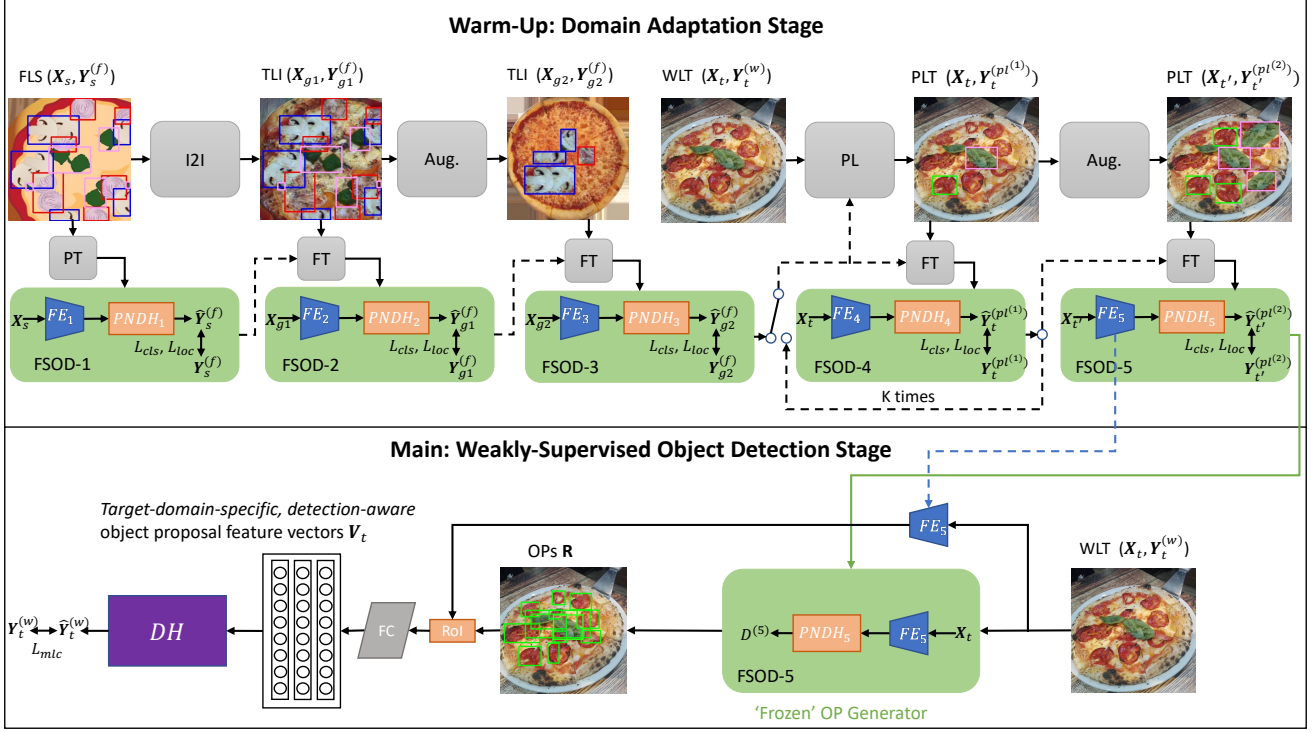


Figure 2: An overview of our Dual-Domain Fully-to-Weakly Supervised Object Detection Architecture (D^2F2WOD). **Upper block:** warm-up domain adaptation stage; **lower block:** main weakly-supervised object detection stage. Here ‘A- - B’ denotes that the parameters of module B are initialized from module A’s parameters. ‘A — B’ denotes that the output of module A is used as an input of module B or module B directly copies module A’s parameters without further fine-tuning. ‘PNDH’ denotes the proposal networks and detection heads in an FSOD model.

stage for initializing the WSOD model. Our method generalizes across different FSODs. Here, we adopt two architectures for the FSOD model – Faster R-CNN [21] and Sparse DETR [24] from the DETR [4] family of object detectors¹.

3.3.1 Progressive Domain Adaptation.

Directly training the FSOD model on the dual domain is challenging, because of (1) substantial data distribution shift between source (non-photographic images) and target (natural images) domains in both foreground and background, and (2) significant supervision discrepancy between source (fully-labeled) and target (lack of localization information) domains. Inspired by DT+PL [15], we overcome this difficulty by generating an intermediate domain \mathcal{G}_1 and \mathcal{G}_2 with instance-level annotations transferred from the source domain. Correspondingly, we introduce a five-step progressive domain adaptation strategy (upper part in Fig. 2) that first pre-trains the FSOD-1 model on the fully-labeled \mathcal{S} , and gradually fine-tunes it on the transfer-labeled \mathcal{G}_1 and augmented transfer-labeled \mathcal{G}_2 to be FSOD-2 and

FSOD-3, and then on the first-round pseudo-labeled \mathcal{T} and second-round augmented pseudo-labeled \mathcal{T} to be FSOD-4 and FSOD-5.

Automated generation of intermediate domains for initial adaptation. To facilitate the adaptation, a desired property of the intermediate domain should be that *its images are similar to the target images while having accurate localization information*. To this end, we generate the intermediate domain images as composition of photo-realistic, target-like objects guided by the layout of objects in the source images, thus allowing direct transfer of localization annotations from the source images to the generated images.

Specifically, since there are no corresponding image pairs between \mathcal{S} and \mathcal{T} domains, we train CycleGAN [43], an unpaired I2I network, to map source images \mathbf{X}_s to domain \mathcal{G}_1 intermediate to the target \mathcal{T} :

$$\mathbf{X}_{g_1} = f_{\mathcal{S} \rightarrow \mathcal{G}_1}(\mathbf{X}_s), \quad (1)$$

where $\mathbf{X}_{g_1} \in \mathbb{R}^{h \times w \times 3}$ is the image generated by I2I network. Given this I2I mapping, we transfer the labels from instances in \mathbf{X}_s to those in \mathbf{X}_{g_1} as

$$\mathbf{Y}_{g_1}^{(f)} = \mathbf{Y}_s^{(f)} : \quad \mathbf{X}_{g_1} = f_{\mathcal{S} \rightarrow \mathcal{G}_1}(\mathbf{X}_s). \quad (2)$$

¹Sparse DETR enhanced the efficiency of DETR and improved the performance on small objects datasets, and thus we choose Sparse DETR here.

Using the intermediate images \mathbf{X}_{g_1} together with their instance-level annotations $\mathbf{Y}_{g_1}^{(f)}$, we fine-tune the FSOD-1 model, pre-trained on \mathcal{S} , into FSOD-2.

To make \mathbf{X}_{g_1} closer to the \mathbf{X}_t images, we focus on separately bridging the foreground and background gap. Specifically, we employ an object-aware data augmentation based on copy-paste [38] to map \mathbf{X}_{g_1} to \mathbf{X}_{g_2} images. For each \mathbf{X}_{g_1} image, we randomly copy several foreground object instances from \mathcal{G}_1 , with resizing and flipping transformations, and paste them onto the real-world target background images from \mathcal{T} to generate \mathbf{X}_{g_2} . Using the augmented intermediate images \mathbf{X}_{g_2} together with their instance-level annotations $\mathbf{Y}_{g_2}^{(f)}$, we fine-tune the FSOD-2 model to FSOD-3.

Instance-level pseudo-annotation of target images for continual adaptation. While the intermediate domains \mathcal{G}_1 and \mathcal{G}_2 partly bridge the source and target domains, there is still non-negligible domain shift between the intermediate and target domains. For example, the synthesized objects translated via CycleGAN are still different from those in the target images; the layout of objects in the intermediate domain is restrictive to that in \mathcal{S} and lacks the real-world variation in \mathcal{T} . Therefore, to achieve good detection performance on the target domain, we need to further fine-tune the FSOD-3 model on the target domain \mathcal{T} as FSOD-4. For this purpose, we use FSOD-3, initially fine-tuned on \mathcal{G}_2 , to produce instance-level pseudo-annotations $\mathbf{Y}_t^{(pl^{(1)})} = \{(\mathbf{b}_1, c_1), \dots, (\mathbf{b}_{N_t}, c_{N_t})\}$ for each weakly-labeled target (WLT) image \mathbf{X}_t .

Specifically, for each image \mathbf{X}_t , we first obtain the predictions $D^{(3)}$ from the FSOD-3 model:

$$D^{(3)} = \{D_1, \dots, D_C\} = f_{\text{FSOD-3}}(\mathbf{X}_t), \quad (3)$$

where D_j indicates all predictions belonging to class $j \in \{1, \dots, C\}$. $D_j = \{d_1, \dots, d_{N_j}\}$, N_j is the number of class j detections, $d_m = (p_m, \hat{\mathbf{b}}_m, j)$, and $p_m \in \mathbb{R}$ indicates the probability of detection $\hat{\mathbf{b}}_m$ belonging to class j . For each ground-truth object class c , we select the top-1 confident prediction d_q from D_c , and we add $(\hat{\mathbf{b}}_q, c)$ to $\mathbf{Y}_t^{(pl^{(1)})}$:

$$d_q = (p_q, \hat{\mathbf{b}}_q, c) : y_c = 1, \quad q = \underset{m}{\operatorname{argmax}} p_m. \quad (4)$$

The FSOD-3 model is subsequently fine-tuned on the target images \mathbf{X}_t with instance-level pseudo-annotations $\mathbf{Y}_t^{(pl^{(1)})}$ into FSOD-4, finally adapting from the target-like \mathcal{G}_2 to \mathcal{T} . In principle, it can be performed K times to generate instance-level pseudo-annotations $\mathbf{Y}_t^{(pl^{(k)})}$ and adapted into FSOD-(3 + k), where $k \in \{1, \dots, K\}$.

However, the typical number of confident pseudo-labeled instances resulting from the FSOD-3 is insufficient for effective adaptation to the target domain. To add instances annotations, we use the copy-paste augmentations

again to produce those object instances. We repeat the previous step, in which the FSOD-4 model is used to produce instance-level pseudo-annotations $\mathbf{Y}_t^{(pl^{(2)})}$. For each pseudo-labeled instance $(\hat{\mathbf{b}}_q, c)$ in \mathbf{X}_t , we copy and randomly paste it L times as $\{(\hat{\mathbf{b}}_{q_1}, c), \dots, (\hat{\mathbf{b}}_{q_L}, c)\}$ onto the original target image \mathbf{X}_t and produce an augmented image \mathbf{X}_t' with new pseudo-annotations $\mathbf{Y}_t^{(pl^{(2)})}$. The FSOD-4 is subsequently fine-tuned on the augmented targets \mathbf{X}_t' with instance-level pseudo-annotations $\mathbf{Y}_t^{(pl^{(2)})}$ into FSOD-5, thus adapting from \mathcal{T} to the augmented \mathcal{T} .

3.4. Main WSOD Stage: Classification and Localization Refinement of Object Proposals

In the main stage of D²F2WOD, we exploit the FSOD-5 model obtained in the warm-up stage to initialize a WSOD model and train it on the real-world target data. As explained in Sec. 2, an MIL-based WSOD model consists of a FE, an OP generator, and a DH. We initialize the FE of the WSOD model with the FE of the fine-tuned FSOD-5 (blue block in Fig. 2) and continually train it on \mathcal{T} . We replace the standard selective search based OP generator of the WSOD model by the entire fine-tuned FSOD-5 (green block in Fig. 2), which is not trained in the WSOD training procedure. Note that here we treat the detection output of the FSOD-5 as the object proposals of the WSOD. This strategy can be seamlessly applied to different types of WSODs, and here we consider the widely-used OICR [32] and the state-of-the-art CASD [14]. By doing so, our proposed model significantly outperforms existing WSOD methods due to: (1) target-domain-specific pre-trained features, (2) detection-aware pre-trained features, and (3) target-domain-specific object proposals.

Generating object proposals and its features. Given an image \mathbf{X}_t , the OP generator aims to obtain M_t bounding boxes $\mathbf{R} = \{\mathbf{b}_1, \dots, \mathbf{b}_{M_t}\}$ associated with \mathbf{X}_t . To this end, for each image \mathbf{X}_t , we first obtain the predictions $D^{(5)}$ from the fine-tuned FSOD-5 model:

$$D^{(5)} = \{D_1, \dots, D_C\} = f_{\text{FSOD-5}}(\mathbf{X}_t). \quad (5)$$

Given that the number of predictions produced by DETR is much less than that of Faster R-CNN, we adopt different proposal generation strategies. For DETR, all predicted bounding boxes are added to \mathbf{R} . For Faster R-CNN, we select predicted bounding boxes $\hat{\mathbf{b}}_m$ belonging to the ground-truth classes to \mathbf{R} . Using the FE followed by an RoI pooling layer and two fully-connected (FC) layers for the WSOD model, we then obtain d -dimensional object proposal feature vectors $\mathbf{V}_t \in \mathbb{R}^{d \times M_t}$ for each input image \mathbf{X}_t (lower part in Fig. 2).

Classification and localization refinement of object proposals. These object proposal feature vectors \mathbf{V}_t are fed

into the detection head of OICR [32] or CASD [14] to classify and localize objects. Please refer to Appendix A for the details.

4. Experimental Results

Benchmarks. We evaluate our method on five dual-domain image benchmark pairs: SyntheticPizza10 [20] \rightarrow RealPizza10 [20], Clipart1K [15] \rightarrow VOC2007 [7], Watercolor2K [15] \rightarrow VOC2007-sub, Comic2K [15] \rightarrow VOC2007-sub, and Clipart1K \rightarrow MS-COCO-sub [18] datasets. We construct the SyntheticPizza10 dataset from [20] by including single-layer images and removing the pizza base-only images (*i.e.*, without any toppings). RealPizza10 is a subset of the PizzaGAN [20], containing 9,213 real images annotated with 13 toppings. As we use pseudo-labeling, we require the classes in $(\mathcal{S}, \mathcal{T})$ to be the same. Thus, we remove images from the PizzaGAN dataset having only spinach, arugula, or corn, the classes absent from SyntheticPizza10, to construct RealPizza10. Similarly, MS-COCO-sub and VOC2007-sub datasets are constructed by removing images without having at least one class from the \mathcal{S} domains. Please see Appendix B for details.

The number of instances for each class in each pair of datasets is unbalanced. Compared with the other benchmarks, SyntheticPizza10 \rightarrow RealPizza10 are more challenging since all Pizza object instances are quite small and have diverse shape and texture. Although [20] uses a variety of different clip-art images for each topping to obtain the synthetic pizzas as shown in Fig. 3, the number of these ingredient templates is still limited. In a real food image, the shape, color and texture of each ingredient object are dependent on cooking actions. As shown in Fig. 3, for each ingredient, the domain gap between SyntheticPizza10 and RealPizza10 varies. In addition, the gap extends to bases of synthetic and real pizzas, as shown in Fig. 3.

Baselines and Evaluation Procedure. We mainly focus on comparing against the state-of-the-art DAOD baselines (cross-domain): DT+PL [15] and PADOD [12], and widely-used WSOD baselines (single-domain): OICR [32], CASD [14], and other baselines including WSDN [2], PCL [31], C-MIL [37], WSOD2(+Reg) [39], Pred Net [1], C-MIDN [8], MIST(+Reg) [22], WeakRPN [33], CASD² (training CASD two times: once for proposal and once for object detection), and CASD+W2N [13]. Our evaluation follows the standard detection procedure. We compute Average Precision (AP) and the mean of AP (mAP) as the evaluation metric. A predicted box is treated as a positive example if it has an IOU > 0.5 between ground truth bounding boxes and the predicted box.

Implementation Details. In the warm-up stage, Faster R-CNN [21] and Sparse DETR [24] were used as our FSOD models. For each target image, we generated 438 object

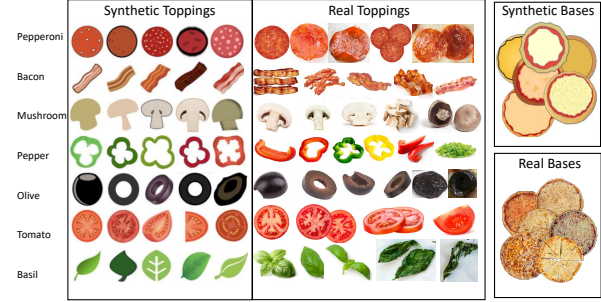


Figure 3: There is a domain shift in toppings and bases of pizzas. Left: Examples of toppings used to create synthetic pizza images [20]. Middle: Examples of toppings in real pizza images. Right top: Examples of bases used to create synthetic pizza images [20]. Right bottom: Examples of bases in real pizza images.

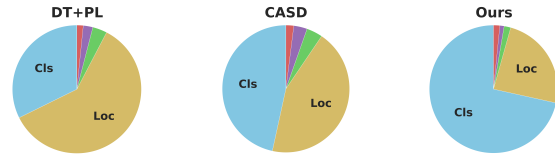


Figure 4: Identify object detection errors.

proposals per image on average on VOC2007 and 441 object proposals per image on average on RealPizza10. Please refer to Appendix C for details.

Source vs. Target Labeling Cost. Two factors determine the trade-off of source vs. target FSOD: the cost of building a synthetic image generator and the realism of the synthesized images. When the realism of the synthetic images is moderate, the cost of building the generator is low. For SyntheticPizza10, built from abstract clipart or patches, the cost of generation is low. Moreover, the annotation of synthetic images is either a byproduct of the generation or inherently easy for human annotators, if such annotation is needed (*e.g.*, Clipart1k). Thus, our approach has inherently lower cost than the direct annotating the target domain.

4.1. Main Results

We compare D²F2WOD with state-of-the-art single (SD) and cross-domain (CD) methods in terms of mAP. Table 1 and Table 2 summarize the detection results on five benchmarks based on Faster R-CNN FSOD backbone. The per class APs are listed in Table 8. D²F2WOD incorporated with OICR is denoted as D²F2WOD_{oicr}, and with CASD is denoted as D²F2WOD_{casd}. The results of our warm-up stage are denoted as D²F2WOD_{warm-up}.

D²F2WOD consistently outperforms the SD baselines. As shown in Table 1, on Clipart1K \rightarrow VOC2007, D²F2WOD_{casd} reaches 64.8% mAP, outperforming the original CASD by 7.8% mAP, and D²F2WOD_{casd+w2n} reaches 66.9% mAP, outperforming the original CASD+W2N by 1.5% mAP, while

Table 1: Results (mAP in %) for different methods on Clipart1K \rightarrow VOC2007. We denote as Upper-Bound the FSOD (Faster R-CNN or Sparse DETR) results, trained and tested on *fully-annotated* target domain to indicate the weak upper-bound performance of our methods. Our warm-up stage is compared with CD models and our main stage is compared with SD models. Faster R-CNN in CD means that we trained our network on fully-annotated source and test on fully-annotated target domains. The best and second best results for D^2F2WOD compared with baselines are shown in red and blue.

		After Warm-Up Stage					After Main Stage												
Type		CD				Ours	SD										Ours		
Method	Upper-Bound	Faster R-CNN [21]	DT+PL [34]	PADOD [12]	$D^2F2WOD_{warm-up}$	WSODN [2]	OICR [32]	PCL [31]	WeakRPN [33]	C-MIL [37]	WSOD2+Reg [39]	Pred Net [1]	C-MIDN [8]	MIST+Reg [22]	CASD [14]	CASD*	CASD+W2N [13]	D^2F2WOD_{casd}	$D^2F2WOD_{casd+win}$
mAP	69.9	22.8	34.6	24.2	37.3	34.8	41.2	43.5	45.3	50.5	53.6	52.9	52.6	54.9	57.0	57.4	65.4	64.8	66.9

Table 2: Results (mAP in %) for different methods on SyntheticPizza10 \rightarrow RealPizza10 (SPizza \rightarrow RPizza), Watercolor2K \rightarrow VOC2007-sub (Water \rightarrow VocS), Comic2K \rightarrow VOC2007-sub (Comi \rightarrow VocS), and Clipart1K \rightarrow MS-COCO-sub (Clip \rightarrow CocoS).

Type	After Warm-Up Stage					After Main Stage			
	Method	Upper-Bound	Faster R-CNN [21]	DT+PL [15]	PADOD [12]	$D^2F2WOD_{warm-up}$	OICR [32]	CASD [14]	D^2F2WOD_{casd}
mAP	SPizza \rightarrow RPizza	-	4.3	14.9	8.1	17.9	4.7	12.9	25.1
	Water \rightarrow VocS	78.0	42.1	49.4	-	52.1	-	65.2	73.2
	Comi \rightarrow VocS	78.0	33.5	46.5	-	49.6	-	65.2	70.8
	Clip \rightarrow CocoS	84.3	13.9	22.1	-	25.7	-	48.3	57.2

CASD² outperforms the original CASD only by 0.4% mAP. The detection performance does not benefit much from using CASD², since doing so does not improve the generated proposals. On SyntheticPizza10 \rightarrow RealPizza10 reported in Table 2, D^2F2WOD_{casd} provides a 12.2% improvement over the original CASD in terms of mAP. **D^2F2WOD also consistently outperforms the CD baselines.** Table 1 shows that on Clipart1K \rightarrow VOC2007 D^2F2WOD_{casd} outperforms DT+PL and PADOD by 30.2% and 40.6% mAP, respectively. As shown in Table 2, D^2F2WOD_{casd} outperforms DT+PL and PADOD on SyntheticPizza10 \rightarrow RealPizza10 by 10.2% and 17.0% mAP, respectively. **D^2F2WOD generalizes across different datasets.** As shown in Table 2, D^2F2WOD effectively handles different domain shifts, successfully leveraging a variety of S^2 .

We observe both stages of D^2F2WOD yield consistently improved detection and localization performance compared with both state-of-the-art SD and CD baselines, especially on the more challenging SyntheticPizza10 \rightarrow RealPizza10 scenario. By exploiting our domain adaptation stage, we believe that our training of the WSOD model is superior to existing methods in three important ways. First, our pre-trained features are target-domain-specific, because of progressive adaptation from source to intermediate to target domains, whereas existing WSOD methods use features pre-trained on ImageNet. Second, our pre-trained features are detection-aware, while ImageNet features used in existing WSOD methods are pre-trained with a single whole-image classification loss, which encourages translation and scale-invariant features. In contrast, the training of our FSOD model involves classification and regression losses, providing features that are sensitive to object locations and scales and are thus useful for detection. Third, our object proposals are target-domain-specific and of high-quality, since they are progressively learned directly on the target domain from foreground and background. Existing WSOD methods

use hand-crafted selective search object proposals, which leads to inaccurate proposals especially for domains such as Pizza, with properties different from VOC2007.

4.2. Ablation Study

We first conducted ablation studies to investigate the effectiveness of our warm-up stage on SyntheticPizza10 \rightarrow RealPizza10 based on the Faster R-CNN FSOD backbone.

Effectiveness of Progressive Adaptation. In our warm-up stage, each adaptation stage (from FSOD-2 to FSOD-5) provides an improvement of 5.4, 0.6, 4.7, 2.9% compared with the previous step in terms of mAP, respectively. Therefore, each adaptation step in our warm-up stage is helpful.

Impact of Adaptation Order. It is important *when* to use copy-paste augmentation. Starting from the same baseline model FSOD-1, if we sequentially fine-tune the FSOD-1 model on intermediate domain \mathcal{G}_1 and augmented intermediate domain \mathcal{G}_2 , the detection performance will be improved by 6.0% mAP from FSOD-1 to FSOD-3. However, if we sequentially fine-tune the FSOD-1 model on augmented intermediate domain \mathcal{G}_2 and intermediate domain \mathcal{G}_1 , the detection performance will be improved by only 1.6% mAP from FSOD-1 to FSOD-3. Similarly, starting from the same FSOD-3 model, if we sequentially fine-tune the FSOD-3 model on first-round pseudo-labeled domain \mathcal{T} and second-round augmented pseudo-labeled domain \mathcal{T} , the detection performance will be improved 7.6% mAP from FSOD-3 to FSOD-5. However, if we sequentially fine-tune the FSOD-3 model on augmented first-round pseudo-labeled domain \mathcal{T} and second-round pseudo-labeled domain \mathcal{T} , the detection performance will be improved by 7.0% mAP from FSOD-3 to FSOD-5.

Generalizability of the Warm-up Stage across FSODs.

We investigate our warm-up stage on other FSOD models such as Sparse DETR on SyntheticPizza10 \rightarrow RealPizza10 datasets. Compared with Faster R-CNN backbone, our $D^2F2WOD_{warm-up}$ and D^2F2WOD_{casd} based on Sparse DETR yields 0.6% and 1.1% improvement in terms of mAP, respectively. These results emphasize the generality of our

²Resource constraints limit our focus on best select SOTA, with extensive comparison delegated to Clipart1K \rightarrow VOC2007 evaluation.

Table 3: Ablation study of D^2F2WOD main configurations on Clipart1K \rightarrow VOC2007 and SyntheticPizza10 \rightarrow RealPizza10.

Type	Method	mAP	
		Clip \rightarrow Voc	SPizza \rightarrow RPizza
SD	OICR	41.2	4.7
	+FE	44.7	8.5
	+OP	47.2	12.6
	+FE+OP	52.7	13.8
SD	CASD	57.0	12.9
	+FE	60.0	14.8
	+OP	60.1	24.0
	+FE+OP	64.8	25.1

framework across different FSOD models. We also conduct ablation studies to investigate the effectiveness of our architecture components in the main FSOD stage, including the domain specific pre-trained deep FE and the weakly-supervised OP generator, as well as the generalization ability of our framework on two WSODs: OICR and CASD. We perform experiments on Clipart1K \rightarrow VOC2007 and SyntheticPizza10 \rightarrow RealPizza10. We find that: (1) our domain specific pre-trained deep FE and weakly-supervised OP generator are both necessary for D^2F2WOD ; and (2) D^2F2WOD can generalize to different WSOD methods.

Main Stage Configurations. From Table 3, we observe that compared with the single-domain baseline networks (OICR and CASD), replacing the VGG16 backbone pre-trained on ImageNet with **domain specific pre-trained deep FE** can improve the performance on VOC2007 (mAP from 41.2% to 44.7%, and from 57.0% to 60.0%, respectively), and on RealPizza10 a consistent improvement is achieved with 3.8% and 1.9% for OICR and CASD, respectively. From Table 1, we observe that our object proposal generator is also better than WeakRPN [33], including a two-stage region proposal network. These results confirm the necessity of the domain-specific pre-trained deep features. Table 3 also shows the impact of the **weakly-supervised OP generator**; it achieves consistent improvements of 3.1% and 11.1%, compared with CASD, on VOC2007 and RealPizza10 datasets, respectively. Together, **FE+OP** results in Table 3 suggest that these two key components are both effective and complementary to each other.

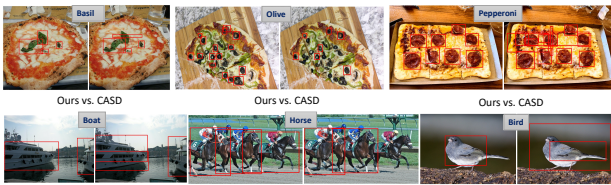


Figure 5: Example of success cases for our D^2F2WOD_{casd} vs. CASD in the test set of RealPizza10 and VOC2007 datasets. We only show instances with scores over 0.3 to maintain visibility.

Generalizability of D^2F2WOD across WSODs. We investigate the impact of our framework as a function of different WSOD methods (here, OICR and CASD). Results in Table 3 emphasize the **generalizability of D^2F2WOD across**

WSODs. The performance gain is observed in both OICR and CASD on the two datasets. The effect of D^2F2WOD is particularly significant for CASD on RealPizza10, since our object proposals are target domain-specific and of high-quality. By contrast, existing WSOD methods use hand-crafted selective search to generate object proposals, leading to inaccurate proposals especially for domains such as Pizza that are very dissimilar to VOC2007.

Identifying Object Detection Errors. We use TIDE [3] to understand the **classification**, **localization**, **both CIs and Loc**, **duplicate detection**, **background**, and **missed GT** errors in our model. As shown in Fig. 4, D^2F2WOD effectively reduces the localization error. Please see Appendix E for more details.

4.3. Qualitative Analysis

Fig. 5 illustrates the detection results produced by our D^2F2WOD and CASD on RealPizza10 and VOC2007 datasets, respectively. There, it can be observed that D^2F2WOD does not only locate most objects, but that it also produces more accurate bounding boxes. Specifically, in the RealPizza10 images it can be appreciated bounding boxes provided by our method (left) closely align with the objects of interest, while for CASD (right) bounding boxes are often imprecise (either wrong shape or big/small). Similar observations can be made for VOC2007 where CASD often fails to locate objects or produces spurious bounding boxes.

5. Discussion and Conclusion

We propose D^2F2WOD , a simple yet effective object generation strategy that can be applied to different WSOD methods. The key insight is to cast WSOD as a domain adaptation problem and improve performance by progressive foreground-background focused transfer learning of an FSOD from non-photographic source to real-world target domains. Empirical evaluation shows D^2F2WOD significantly outperforms state of the art on several benchmarks.

Limitation. Our framework requires extra training time for CycleGAN, which brings in the most additional computation overhead. While D^2F2WOD offers a promising way to solve WSOD in the presence of a large domain gap, it currently lacks the ability to jointly learn and refine all stages in the pipeline. An end-to-end large-gap WSOD could offer additional improvement in detection performance on the target domain through creation of increasingly discriminative object features. However, one challenge with that setting would be to control the back-propagation of possible errors induced by the PL steps.

Acknowledgement. This work was supported in part by NSF IIS Grant #1955404.

References

- [1] Aditya Arun, CV Jawahar, and M Pawan Kumar. Dissimilarity coefficient based weakly supervised object detection. In *CVPR*, 2019. 2, 6, 7, 15
- [2] Hakan Bilen and Andrea Vedaldi. Weakly supervised deep detection networks. In *CVPR*, 2016. 1, 2, 6, 7, 15
- [3] Daniel Bolya, Sean Foley, James Hays, and Judy Hoffman. Tide: A general toolbox for identifying object detection errors. In *ECCV*, 2020. 8, 15
- [4] Nicolas Carion, Francisco Massa, Gabriel Synnaeve, Nicolas Usunier, Alexander Kirillov, and Sergey Zagoruyko. End-to-end object detection with transformers. In *ECCV*, 2020. 1, 2, 3, 4
- [5] Yuhua Chen, Wen Li, Christos Sakaridis, Dengxin Dai, and Luc Van Gool. Domain adaptive faster r-cnn for object detection in the wild. In *CVPR*, 2018. 3
- [6] Thomas G Dietterich, Richard H Lathrop, and Tomás Lozano-Pérez. Solving the multiple instance problem with axis-parallel rectangles. *Artificial intelligence*, 89(1-2):31–71, 1997. 1
- [7] Mark Everingham, Luc Van Gool, Christopher KI Williams, John Winn, and Andrew Zisserman. The pascal visual object classes (voc) challenge. *IJCV*, 88(2):303–338, 2010. 6, 12
- [8] Yan Gao, Boxiao Liu, Nan Guo, Xiaochun Ye, Fang Wan, Haihang You, and Dongrui Fan. C-midn: Coupled multiple instance detection network with segmentation guidance for weakly supervised object detection. In *ICCV*, 2019. 1, 2, 6, 7, 15
- [9] Golnaz Ghiasi, Yin Cui, Aravind Srinivas, Rui Qian, Tsung-Yi Lin, Ekin D Cubuk, Quoc V Le, and Barret Zoph. Simple copy-paste is a strong data augmentation method for instance segmentation. In *CVPR*, 2021. 2, 3
- [10] Ross Girshick. Fast r-cnn. In *ICCV*, 2015. 2
- [11] Kaiming He, Xiangyu Zhang, Shaoqing Ren, and Jian Sun. Deep residual learning for image recognition. In *CVPR*, 2016. 12
- [12] Han-Kai Hsu, Chun-Han Yao, Yi-Hsuan Tsai, Wei-Chih Hung, Hung-Yu Tseng, Maneesh Singh, and Ming-Hsuan Yang. Progressive domain adaptation for object detection. In *WACV*, 2020. 3, 6, 7, 15
- [13] Zitong Huang, Yiping Bao, Bowen Dong, Erjin Zhou, and Wangmeng Zuo. W2n: Switching from weak supervision to noisy supervision for object detection. In *ECCV*, 2022. 2, 6, 7, 15
- [14] Zeyi Huang, Yang Zou, BVK Kumar, and Dong Huang. Comprehensive attention self-distillation for weakly-supervised object detection. In *NeurIPS*, 2020. 1, 2, 3, 5, 6, 7, 11, 12, 13, 15
- [15] Naoto Inoue, Ryosuke Furuta, Toshihiko Yamasaki, and Kiyoharu Aizawa. Cross-domain weakly-supervised object detection through progressive domain adaptation. In *CVPR*, 2018. 1, 3, 4, 6, 7, 12, 13, 15
- [16] Seunghyeon Kim, Jaehoon Choi, Taekyung Kim, and Chang-ick Kim. Self-training and adversarial background regularization for unsupervised domain adaptive one-stage object detection. In *ICCV*, 2019. 3
- [17] Dong-Hyun Lee et al. Pseudo-label: The simple and efficient semi-supervised learning method for deep neural networks. In *ICML Workshop*, 2013. 2
- [18] Tsung-Yi Lin, Michael Maire, Serge Belongie, James Hays, Pietro Perona, Deva Ramanan, Piotr Dollár, and C Lawrence Zitnick. Microsoft coco: Common objects in context. In *ECCV*, 2014. 6, 12
- [19] Minh Hoai Nguyen, Lorenzo Torresani, Fernando De La Torre, and Carsten Rother. Weakly supervised discriminative localization and classification: a joint learning process. In *ICCV*, 2009. 2
- [20] Dim P Papadopoulos, Youssef Tamaazousti, Ferda Ofli, Ingmar Weber, and Antonio Torralba. How to make a pizza: Learning a compositional layer-based gan model. In *CVPR*, 2019. 1, 6, 12
- [21] Shaoqing Ren, Kaiming He, Ross Girshick, and Jian Sun. Faster r-cnn: Towards real-time object detection with region proposal networks. In *NeurIPS*, 2015. 1, 2, 3, 4, 6, 7, 13, 15
- [22] Zhongzheng Ren, Zhiding Yu, Xiaodong Yang, Ming-Yu Liu, Yong Jae Lee, Alexander G Schwing, and Jan Kautz. Instance-aware, context-focused, and memory-efficient weakly supervised object detection. In *CVPR*, 2020. 1, 2, 6, 7, 11, 15
- [23] Adrian Lopez Rodriguez and Krystian Mikolajczyk. Domain adaptation for object detection via style consistency. *arXiv preprint arXiv:1911.10033*, 2019. 3
- [24] Byungseok Roh, JaeWoong Shin, Wuhyun Shin, and Sae-hoon Kim. Sparse detr: Efficient end-to-end object detection with learnable sparsity. In *ICLR*, 2022. 4, 6, 13
- [25] Aruni RoyChowdhury, Prithvijit Chakrabarty, Ashish Singh, SouYoung Jin, Huaizu Jiang, Liangliang Cao, and Erik Learned-Miller. Automatic adaptation of object detectors to new domains using self-training. In *CVPR*, 2019. 3
- [26] Olga Russakovsky, Jia Deng, Hao Su, Jonathan Krause, Sanjeev Satheesh, Sean Ma, Zhiheng Huang, Andrej Karpathy, Aditya Khosla, Michael Bernstein, et al. Imagenet large scale visual recognition challenge. *IJCV*, 115(3):211–252, 2015. 12
- [27] Kuniaki Saito, Yoshitaka Ushiku, Tatsuya Harada, and Kate Saenko. Strong-weak distribution alignment for adaptive object detection. In *CVPR*, 2019. 3
- [28] Karen Simonyan and Andrew Zisserman. Very deep convolutional networks for large-scale image recognition. In *ICLP*, 2015. 12
- [29] Vishwanath A Sindagi, Poojan Oza, Rajeesh Yasarla, and Vishal M Patel. Prior-based domain adaptive object detection for hazy and rainy conditions. In *ECCV*, 2020. 3
- [30] Christian Szegedy, Wei Liu, Yangqing Jia, Pierre Sermanet, Scott Reed, Dragomir Anguelov, Dumitru Erhan, Vincent Vanhoucke, and Andrew Rabinovich. Going deeper with convolutions. In *CVPR*, 2015. 3
- [31] Peng Tang, Xinggang Wang, Song Bai, Wei Shen, Xiang Bai, Wenyu Liu, and Alan Yuille. Pcl: Proposal cluster learning for weakly supervised object detection. *TPAMI*, 42(1):176–191, 2018. 1, 2, 6, 7, 15
- [32] Peng Tang, Xinggang Wang, Xiang Bai, and Wenyu Liu. Multiple instance detection network with online instance

- classifier refinement. In *CVPR*, 2017. 1, 2, 3, 5, 6, 7, 11, 12, 13, 15
- [33] Peng Tang, Xinggang Wang, Angtian Wang, Yongluan Yan, Wenyu Liu, Junzhou Huang, and Alan Yuille. Weakly supervised region proposal network and object detection. In *ECCV*, 2018. 2, 6, 7, 8, 15
 - [34] Jasper RR Uijlings, Koen EA Van De Sande, Theo Gevers, and Arnold WM Smeulders. Selective search for object recognition. *IJCV*, 104(2):154–171, 2013. 1, 2
 - [35] Nanne Van Noord and Eric Postma. Learning scale-variant and scale-invariant features for deep image classification. *Pattern Recognition*, 61:583–592, 2017. 2
 - [36] Vibashan VS, Vikram Gupta, Poojan Oza, Vishwanath A Sindagi, and Vishal M Patel. Mega-cda: Memory guided attention for category-aware unsupervised domain adaptive object detection. In *CVPR*, 2021. 3
 - [37] Fang Wan, Chang Liu, Wei Ke, Xiangyang Ji, Jianbin Jiao, and Qixiang Ye. C-mil: Continuation multiple instance learning for weakly supervised object detection. In *CVPR*, 2019. 1, 2, 6, 7, 15
 - [38] Sangdoo Yun, Dongyoon Han, Seong Joon Oh, Sanghyuk Chun, Junsuk Choe, and Youngjoon Yoo. Cutmix: Regularization strategy to train strong classifiers with localizable features. In *ICCV*, 2019. 2, 3, 5, 13
 - [39] Zhaoyang Zeng, Bei Liu, Jianlong Fu, Hongyang Chao, and Lei Zhang. Wsod2: Learning bottom-up and top-down objectness distillation for weakly-supervised object detection. In *ICCV*, 2019. 2, 6, 7, 11, 15
 - [40] Ming Zhang, Shuaicheng Liu, and Bing Zeng. Hierarchical region proposal refinement network for weakly supervised object detection. In *ICIP*, 2021. 2
 - [41] Zhi Zhang, Tong He, Hang Zhang, Zhongyue Zhang, Junyuan Xie, and Mu Li. Bag of freebies for training object detection neural networks. *arXiv preprint arXiv:1902.04103*, 2019. 3
 - [42] Ganlong Zhao, Guanbin Li, Ruijia Xu, and Liang Lin. Collaborative training between region proposal localization and classification for domain adaptive object detection. In *ECCV*, 2020. 3
 - [43] Jun-Yan Zhu, Taesung Park, Phillip Isola, and Alexei A Efros. Unpaired image-to-image translation using cycle-consistent adversarial networks. In *ICCV*, 2017. 2, 4, 13
 - [44] C Lawrence Zitnick and Piotr Dollár. Edge boxes: Locating object proposals from edges. In *ECCV*, 2014. 1, 2

A. Details of WSOD Models

Our object proposal generation strategy can be applied to different WSOD methods to boost their detection performance. In the main paper, we show two representative WSOD models – the widely-used OICR [32] and the state-of-the-art CASD [14]. Here, we highlight the main modeling elements of OICR and CASD. Additional details can be found in [32, 14].

As mentioned in Sec. 3.4 of the main paper, we obtain d -dimensional object proposal feature vectors $\mathbf{V}_t \in \mathbb{R}^{d \times M_t}$ for each input image \mathbf{X}_t , where M_t is the number of the proposal bounding boxes associated with \mathbf{X}_t . These object features are fed into the detection head of OICR [32] or CASD [14] to classify and localize objects. Both models contain a core multiple instance detection network (MIL) and P instance refinement classifiers.

A.1. Core MIL Head

As shown in Fig. 6, the core multiple instance detection network conducts the image-level multiple instance classification supervised by image-level labels $\mathbf{Y}_t^{(w)}$. In the core multiple instance detection network, the object proposal feature vectors \mathbf{V}_t of image \mathbf{X}_t are branched into two parallel classification and detection streams to generate two matrices $\mathbf{x}^{(\text{cls})}$ and $\mathbf{x}^{(\text{det})} \in \mathbb{R}^{C \times M_t}$ by two FC layers, where C is number of classes in \mathcal{T} . Then, $\mathbf{x}^{(\text{cls})}$ passes through a softmax layer along the category direction (column-wise), while $\mathbf{x}^{(\text{det})}$ passes through another softmax layer along the proposal direction (row-wise), leading to $\sigma(\mathbf{x}^{(\text{cls})})$ and $\sigma(\mathbf{x}^{(\text{det})})$, respectively. The instance-level classification score for the object proposals is computed as the element-wise product $\mathbf{x}^{(0)} = \sigma(\mathbf{x}^{(\text{cls})}) \odot \sigma(\mathbf{x}^{(\text{det})})$. Finally, the image-level classification score for class c is obtained as $p_c = \sum_{i=1}^{M_t} \mathbf{x}_{c,i}^{(0)}$. We train the core instance classifier using a multi-class cross-entropy loss \mathcal{L}_{mlc} . By using the instance-level classification scores $\mathbf{x}^{(0)}$, we select proposals as detected objects. However, the core MIL head focuses on most discriminative object instances.

A.2. OICR

To address this issue, OICR [32] introduces multi-stage instance refinement classifiers to refine the core instance classifier. As shown in Fig. 6, \mathbf{V}_t is fed into P refinement instance classifiers. Each p -th refinement classifier comprises of an FC and a softmax layers along the category direction, and produces a proposal score matrix $\mathbf{x}^{(p)} \in \mathbb{R}^{(C+1) \times M_t}$, where the $(C+1)$ -th category is the background class. We train the p -th refinement instance classifier via a log loss $\mathcal{L}_{\text{ref}}^p$ supervised by instance-level pseudo-labels, which are selected from the top-scoring proposals in the previous stage.

The loss for training the OICR network $\mathcal{L}_{\text{oicr}}$ is defined

as

$$\mathcal{L}_{\text{oicr}} = \mathcal{L}_{\text{mlc}} + \lambda_d \sum_{p=1}^P \mathcal{L}_{\text{ref}}^p, \quad (6)$$

where λ_d is the trade-off hyperparameter.

A.3. CASD

To further improve OICR, CASD [14] employs an attention-based feature learning method for WSOD model training. In addition to the $\mathcal{L}_{\text{oicr}}$ loss, CASD includes a proposal bounding box smooth \mathcal{L}_1 regression loss $\mathcal{L}_{\text{reg}}^p$ for p -th refinement instance classifier by following [39, 22].

To encourage consistent representation learning of the same image under different transformations (horizontal flipping and scaling), we consider the Input-wise CASD following [14]. For each image \mathbf{X}_t , we construct a set of images $\mathbf{X}_t^{tr} = \{\mathbf{X}_t^{(s1)}, \mathbf{X}_t^{(\text{flip}(s1))}, \dots, \mathbf{X}_t^{(sn)}, \mathbf{X}_t^{(\text{flip}(sn))}\}$, where $\mathbf{X}_t^{(si)}$ is its scaled image at si scale, $\mathbf{X}_t^{(\text{flip}(si))}$ is the horizontally flipped image of the scaled image, and n is the number of scales. Then, by feeding the set of images \mathbf{X}_t^{tr} into the same feature extractor FE_5 in the WSOD model, we obtain a set of image feature maps $\mathbf{F}_t^{tr} = \{\mathbf{F}_t^{(s1)}, \mathbf{F}_t^{(\text{flip}(s1))}, \dots, \mathbf{F}_t^{(sn)}, \mathbf{F}_t^{(\text{flip}(sn))}\}$. For each object proposal r , we compute the proposal feature vectors cropped from \mathbf{F}_t^{tr} , and use all proposal feature vectors to obtain a set of object proposal attention maps $\mathbf{A}_r^{tr} = \{\mathbf{A}_r^{(s1)}, \mathbf{A}_r^{(\text{flip}(s1))}, \dots, \mathbf{A}_r^{(sn)}, \mathbf{A}_r^{(\text{flip}(sn))}\}$ by channel-wise average pooling and element-wise sigmoid function. We use the aggregated attention maps $\mathbf{A}_r^{IW} = \max(\mathbf{A}_r^{tr})$, where $\max(\cdot)$ is the element-wise max operator, to update the feature extractor FE_5 in the p -th refinement step. During training, we add the $\mathcal{L}_{\text{IW}}^p$ loss, which is an \mathcal{L}_2 loss between \mathbf{A}_r^{IW} and each object proposal attention map in \mathbf{A}_r^{tr} .

To encourage balanced representation learning of the same image produced at different feature extractor layers, we consider the Layer-wise CASD following [14]. The feature extractor FE_5 consists of Q number of convolutional blocks $FE_5 = \{B_1, \dots, B_Q\}$. The original image \mathbf{X}_t is fed into each of them to output a set of feature map $\mathbf{F}_t^B = \{\mathbf{F}_t^{B_1}, \dots, \mathbf{F}_t^{B_Q}\}$. For each object proposal r , we compute the proposal feature vector in each block and use all the feature vectors to obtain a set of object proposal attention maps $\mathbf{A}_r^{bl} = \{\mathbf{A}_r^{B_1}, \dots, \mathbf{A}_r^{B_Q}\}$. Similarly to Input-wise CASD, we obtain the aggregated attention maps $\mathbf{A}_r^{LW} = \max(\mathbf{A}_r^{bl})$. To update the feature extractor FE_5 in the p -th refinement step, we add the $\mathcal{L}_{\text{LW}}^p$ loss, which is an \mathcal{L}_2 loss between \mathbf{A}_r^{LW} and each object proposal attention map in \mathbf{A}_r^{bl} .

The loss for training the CASD network $\mathcal{L}_{\text{casd}}$ is defined

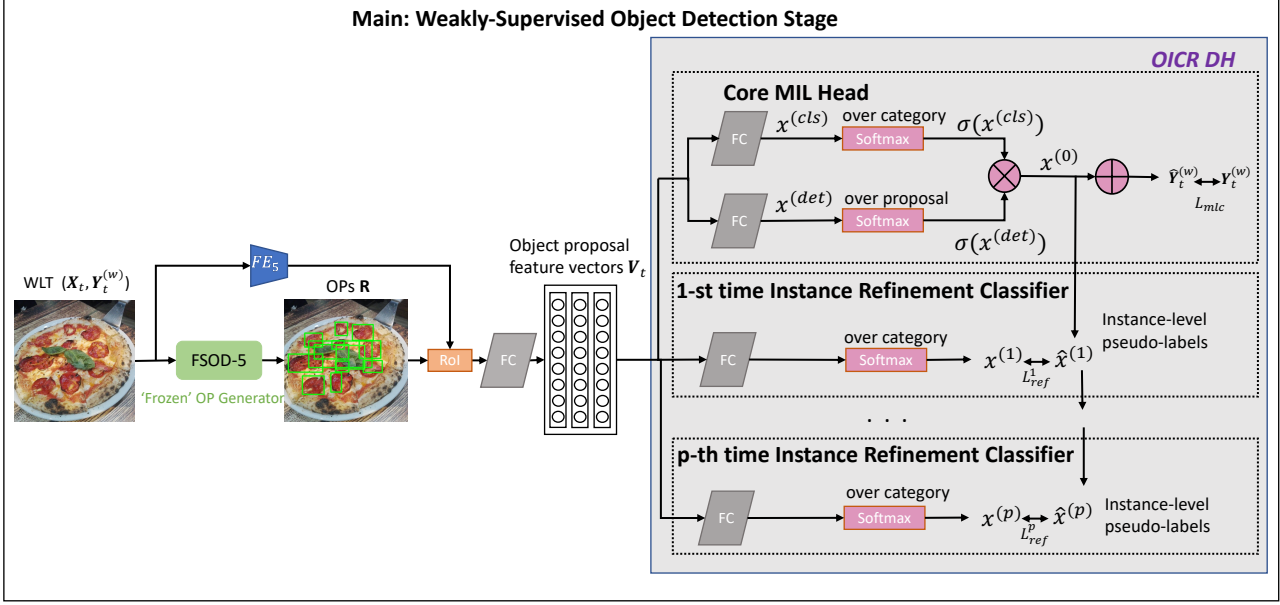


Figure 6: The architecture of our main weakly-supervised object detection stage.

as

$$\mathcal{L}_{\text{casd}} = \mathcal{L}_{\text{mlc}} + \sum_{p=1}^P (\lambda_d \mathcal{L}_{\text{ref}}^p + \lambda_g \mathcal{L}_{\text{reg}}^p + \lambda_i \mathcal{L}_{\text{IW}}^p + \lambda_l \mathcal{L}_{\text{LW}}^p), \quad (7)$$

where λ_d , λ_g , and λ_i are the trade-off hyperparameters. For additional details please refer to [32, 14].

B. Benchmarks

We evaluate our method on five dual-domain image benchmark pairs: SyntheticPizza10 [20] \rightarrow RealPizza10 [20], Clipart1K [15] \rightarrow VOC2007 [7], Watercolor2K [15] \rightarrow VOC2007-sub, Comic2K [15] \rightarrow VOC2007-sub, and Clipart1K \rightarrow MS-COCO-sub [18] datasets. Each synthetic pizza contains up to 10 toppings. The total 16,340 SyntheticPizza10 images are split into 14,802 training and 1,538 testing. RealPizza10 is split into 5,029 training and 552 testing images. Both Clipart1K and VOC2007 contain 20 object classes. Both Watercolor2K and Comic2K contain 6 classes: bike, bird, car, cat, dog, and person, the subset of classes in the VOC2007. The Watercolor2K and Comic2K domains are split into two subsets: 1,000 training and 1,000 testing images. The VOC2007-sub dataset includes 3,487 training and 3,457 testing images. The MS-COCO-sub domain includes 95,279 training images and 4,031 testing images.

Challenge of SyntheticPizza10 \rightarrow RealPizza10 benchmark. One of our contributions is that we construct the dual-domain benchmark SyntheticPizza10 \rightarrow RealPizza10 for WSOD. Compared with existing WSOD benchmarks

(VOC2007 and MS-COCO), RealPizza10 is more challenging for the following reasons. First, there are more objects per image. On RealPizza10 each image contains 20 objects on average, while on VOC2007 there are 2 objects per image on average. Second, there is strong variation in appearance. For example, the toppings in Pizza images exhibit complex changes in appearance. Third, there are layered object occlusions due to the topping objects. Such difficulty is further reflected in the low detection performance of baselines on RealPizza10 (e.g., Faster R-CNN achieves only 4.3% mAP on RealPizza10, while 22.8% mAP on VOC2007 and 13.9% mAP on MS-COCO-sub, as shown in Tables 1 and 2 in the main paper). We hope Pizza10 can serve as a new WSOD benchmark.

C. Additional Implementation Details

Implementation Details. All models and experiments were implemented in Pytorch. The VGG16 [28] and ResNet-50 [11] models pre-trained on ImageNet [26] were used as FSOD feature extractor and WSOD feature extractor. VGG16 was used as Faster R-CNN feature extractor and ResNet-50 was used as Sparse DETR feature extractor. Because VOC2007 and MS-COCO lack clean background, we run experiments on Clipart1K \rightarrow VOC2007, Watercolor2K \rightarrow VOC2007-sub, Comic2K \rightarrow VOC2007-sub, and Clipart1K \rightarrow MS-COCO-sub without the 3rd adaptation step FSOD-3 on augmented intermediate domain \mathcal{G}_2 in our warm-up stage.

In the main stage, the maximum number of training iteration was set to be 100K for all target domains.

Copy-Paste Augmentation. As stated in Sec. 3.3 of the main paper, we employ an object-aware data augmentation method based on copy-paste [38] to map images \mathbf{X}_{g_1} to \mathbf{X}_{g_2} . For each image \mathbf{X}_{g_1} , we randomly copy several foreground object instances from \mathcal{G}_1 , with resizing and flipping transformations, and paste them onto the real-world target background images from \mathcal{T} to generate \mathbf{X}_{g_2} . The flipping transformation includes horizontal and vertical flipping transformations. The resize ratio is a random value between 0.8 to 1.2. The PL step can be in principle performed for K times to generate instance-level pseudo-annotations. In our experiments, we found that running the PL step twice has achieved satisfactory performance. After the second PL step, we apply the copy-paste augmentation with resizing and flipping transformations for the pseudo-labeled target images. According to the statistic information of Clipart1k \rightarrow VOC2007 reported in Table 4, for each class, there is a maximum of two objects in an image. Therefore, we copy each pseudo-labeled object and randomly paste it 0 or 1 time onto the original image. On SyntheticPizza10 \rightarrow RealPizza10, according to the statistic information reported in Table 5, we copy each pseudo-labeled object and randomly paste it maximum 20 times onto the original image. All the pasted objects and original objects have no overlapping.

CycleGAN. We trained CycleGAN [43] with the learning rate of 1.0×10^{-5} for the first ten epochs and a linear decaying rate to zero over the next ten epochs following [15] to generate intermediate images. We followed the original paper [43] for remaining hyperparameters.

Faster R-CNN. We trained Faster R-CNN [21] on images of a single scale. The short edge of input images was rescaled to 600, and the longest image edge was capped to 1000. We employed a learning rate, which is the same as the final learning rate for the previous step, to progressively fine-tune Faster R-CNN on (1) a transfer-labeled intermediate domain \mathcal{G}_1 , (2) augmented transfer-labeled intermediate domain \mathcal{G}_2 and then on (3) the pseudo-labeled target domain \mathcal{T} and (4) augmented pseudo-labeled target domain \mathcal{T} .

Sparse DETR. The number of object queries is 300 and we only use 10% of the encoder tokens on all benchmarks. We followed the original paper [24] for the other hyperparameters. Each adaptation step was conducted with the learning rate equal to the final learning rate of the prior step.

OICR and CASD. We followed the original papers [32, 14] for the hyperparameters.

Object Proposals. The number of instances for each class in SyntheticPizza10 \rightarrow RealPizza10 and Clipart1K \rightarrow

VOC2007 is unbalanced and the statistics information is reported in Table 4 and Table 5, respectively. The statistics information of object proposals mentioned in the main paper is shown in Table 6.

Cost of Training and Computing Resources. We train D^2F2WOD based on Faster R-CNN on a Tesla K80 GPU. As shown in Table 7, we have the following observations. (1) The warm-up stage takes much less time than the main stage, indicating our domain adaptation to be lightweight. (2) Standard CycleGAN training brings in the most additional computation overhead.

D. Additional Main Results

In Sec. 4.1 of the main paper we show the main results based on mAP values. Here, we list the whole mAP with per class AP values. Table 8a and Table 8b summarize the detection results on Clipart1K \rightarrow VOC2007 and SyntheticPizza10 \rightarrow RealPizza10 based on Faster R-CNN FSOD backbone, respectively. D^2F2WOD incorporated with OICR is denoted as D^2F2WOD_{oicr} , with CASD is denoted as D^2F2WOD_{casd} , and with CASD+W2N is denoted as $D^2F2WOD_{casd+w2n}$. The results of our warm-up stage are denoted as $D^2F2WOD_{warm-up}$.

The detection performance does not benefit from using OICR or CASD twice (once for proposal and once for object detection), since doing so does not improve the generated proposals. The result of training CASD two times is denoted as $CASD^2$. As shown in Table 8a, on Clipart1K \rightarrow VOC2007, D^2F2WOD_{casd} reaches 64.8% mAP, outperforming the original CASD by 7.8% mAP, while $CASD^2$ reaches 57.4% mAP, outperforming the original CASD by 0.4% mAP. The detection result of using OICR twice will be the same as using OICR once, because OICR directly uses the proposals produced by selective search without refinement on their bounding boxes. $D^2F2WOD_{casd+w2n}$ reaches 66.9% mAP, outperforming the original CASD+W2N by 1.5% mAP. This further validates that D^2F2WOD is a general framework that can be combined with different WSOD methods to improve their object proposal generation and thus overall performance.

E. Additional Ablation Study

In Sec. 4.2 of the main paper we show the ablation study results based on the mAP values. Here, we list the whole mAP values with per class AP values.

- **Effectiveness of Progressive Adaptation.** As shown in Table 9, each adaptation step in our warm-up stage is not only helpful in terms of mAP, but it also benefits for each class.

Table 4: Statistics of Clipart1k \rightarrow VOC2007 (train+test): number of images (#img), number of instances (#ins), and relative size of human-labeled object instances on average (%size).

Name	Clipart			VOC			Name	Clipart			VOC		
	#img	#ins	%size	#img	#ins	%size		#img	#ins	%size	#img	#ins	%size
Aero	41	73	14.7	442	591	26.3	Table	106	115	19.7	390	421	33.3
Bike	27	36	20.1	482	690	22.0	Dog	51	54	9.2	839	999	34.1
Bird	135	265	9.4	612	945	20.2	Horse	46	79	17.4	561	710	30.2
Boat	88	129	12.1	353	553	17.2	Mbike	16	17	51.2	467	664	28.3
Bottle	60	121	3.5	456	974	5.8	Person	521	1185	14.5	4015	9218	16.5
Bus	20	21	31.7	360	442	28.9	Plant	100	178	5.6	469	994	11.6
Car	103	202	11.0	1434	2451	19.8	Sheep	27	76	8.1	193	499	13.0
Cat	43	50	8.4	659	734	41.9	Sofa	42	52	19.1	452	487	35.6
Chair	181	340	8.6	862	1554	12.2	Train	45	46	40.3	520	579	36.9
Cow	30	46	19.1	268	503	18.4	Tv	65	80	8.4	485	632	12.8
Total								1000	3165	12.9	9963	24640	19.9

Table 5: Statistics of SyntheticPizza10 (train+test) \rightarrow RealPizza10 (only test set is annotated, so here we report test statistic): number of images (#img), number of instances (#ins), and relative size of human-labeled object instances on average (%size).

Dataset	Pepperoni	Mushroom	Pepper	Olive	Basil	Bacon	Broccoli	Pineapple	Tomato	Onion	Total
Synthetic	#img	3741	3894	3901	3729	3868	3725	3904	3638	3979	16340
	#ins	29113	31723	29336	29001	36846	36113	31853	28675	31374	313595
	%size	2.4	2.2	2.4	2.4	1.4	1.3	2.2	2.3	2.3	2.1
Real	#img	197	96	94	70	152	24	10	8	161	552
	#ins	3638	1455	1239	841	1145	289	110	152	1697	11272
	%size	1.3	1.0	1.0	0.6	1.4	1.8	1.5	0.9	1.3	1.2

Table 6: Statistical information of the number of object proposals per image generated by the Faster R-CNN backbone in source domains.

Datasets	Min	Max	Mean	Std
PASCAL VOC 2007 train	300.0	1800.0	437.3	195.5
PASCAL VOC 2007 test	300.0	1500.0	424.8	185.0
RealPizza10 2007 train	300.0	1800.0	441.0	225.7
RealPizza10 2007 test	300.0	1500.0	482.6	236.7

Table 7: Training time for different stages on Clipart1K \rightarrow VOC2007 (Clip \rightarrow VOC), SyntheticPizza10 \rightarrow RealPizza10 (SPizza \rightarrow RPizza), Watercolor2K \rightarrow VOC2007-sub (Water \rightarrow VocS), and Comic2K \rightarrow VOC2007-sub (Comi \rightarrow VocS) based on Faster R-CNN FSOD backbone. ‘-’ denotes that we run experiments without the 3rd adaptation step FSOD-3, since VOC2007 and MS-COCO lack clean background.

Training time	Dataset	Warm-Up Stage					Main Stage	CycleGAN
Stage		FSOD-1	FSOD-2	FSOD-3	FSOD-4	FSOD-5	CASD	
hour	SPizza \rightarrow RPizza	14	10	13	2	2	79	216
	Clip \rightarrow Voc	7	6	-	3	3	102	144
	Water \rightarrow VocS	8	8	-	2	2	81	144
	Comi \rightarrow VocS	4	4	-	8	8	81	144

- **Impact of Adaptation Order.** Table 10 shows that our *progressive* adaptation order that gradually reduces domain gap achieves the best performance – it is better to first fine-tune the FSOD on intermediate images or pseudo-labeled images, and then fine-tune on the augmented images.

- **Generalizability of the Warm-up Stage across**

FSODs. As shown in Table 11, our $D^2F2WOD_{warm-up}$ and D^2F2WOD_{casd} based on Sparse DETR yield 0.6% and 1.1% improvement in terms of mAP, respectively, compared with Faster R-CNN backbone.

- **Main Stage Configurations.** As shown in Table 12, two key components of our method are both effective and complementary to each other. Note that the

Table 8: Results (AP in %) for different methods on Clipart1K \rightarrow VOC2007 and SyntheticPizza10 \rightarrow RealPizza10. We denote as Upper-Bound the FSOD (Faster R-CNN or Sparse DETR) results, trained and tested on *fully-annotated* target domain to indicate the weak upper-bound performance of our methods. Our warm-up stage is compared with CD models and our main stage is compared with SD models. The upper part shows the results using CD models. The lower part shows the results using SD methods. Faster R-CNN in CD means we trained our network on fully-annotated source and test on fully-annotated target domains. The best and second best results for D^2F2WOD compared with baselines are shown in red and blue.

(a) Clipart1K \rightarrow VOC2007.																						
Type	Method	mAP	Aero	Bike	Bird	Boat	Bottle	Bus	Car	Cat	Chair	Cow	Table	Dog	Horse	Mbike	Person	Plant	Sheep	Sofa	Train	Tv
CD	Upper-Bound [21]	69.9	69.8	79.1	67.5	56.5	54.4	77.2	82.2	80.9	50.1	78.4	64.5	78.4	83.7	72.3	77.2	38.3	70.9	66.6	77.5	71.9
	Faster R-CNN [21]	22.8	10.7	39.7	30.5	8.6	19.3	27.4	48.0	4.5	23.7	21.2	7.9	19.0	21.9	21.5	45.0	17.4	16.1	22.5	25.5	25.0
	DT+PL [15]	34.6	18.8	55.8	33.2	20.4	18.8	47.2	56.2	15.8	27.4	45.5	10.7	25.9	54.1	54.3	47.6	10.6	35.4	42.3	47.0	25.9
	PADOD [12]	24.2	13.3	40.3	28.8	12.6	20.2	32.2	46.7	7.5	25.9	24.0	13.8	19.3	21.2	17.5	44.0	17.6	17.2	24.4	28.5	29.4
Ours	D ² F2WOD _{warm-up}	37.3	20.7	60.8	37.2	19.4	25.0	51.1	59.7	17.2	30.4	44.4	17.3	27.4	55.8	56.8	47.6	12.9	38.4	45.5	50.3	27.6
SD	WSDN [2]	34.8	39.4	50.1	31.5	16.3	12.6	64.5	42.8	42.6	10.1	35.7	24.9	38.2	34.4	55.6	9.4	14.7	30.2	40.7	54.7	46.9
	OICR [32]	41.2	58.0	62.4	31.1	19.4	13.0	65.1	62.2	28.4	24.8	44.7	30.6	25.3	37.8	65.5	15.7	24.1	41.7	46.9	64.3	62.6
	PCL [31]	43.5	54.4	69.0	39.3	19.2	15.7	62.9	64.4	30.0	25.1	52.5	44.4	19.6	39.3	67.7	17.8	22.9	46.6	57.5	58.6	63.0
	WeakRPN [33]	45.3	57.9	70.5	37.8	5.7	21.0	66.1	69.2	59.4	3.4	57.1	57.3	35.2	64.2	68.6	32.8	28.6	50.8	49.5	41.1	30.0
	C-MIL [37]	50.5	62.5	58.4	49.5	32.1	19.8	70.5	66.1	63.4	20.0	60.5	52.9	53.5	57.4	68.9	8.4	24.6	51.8	58.7	66.7	63.5
	WSOD2(+Reg) [39]	53.6	65.1	64.8	57.2	39.2	24.3	69.8	66.2	61.0	29.8	64.6	42.5	60.1	71.2	70.7	21.9	28.1	58.6	59.7	52.2	64.8
	Pred Net [1]	52.9	66.7	69.5	52.8	31.4	24.7	74.5	74.1	67.3	14.6	53.0	46.1	52.9	69.9	70.8	18.5	28.4	54.6	60.7	67.1	60.4
	C-MIDN [8]	52.6	53.3	71.5	49.8	26.1	20.3	70.3	69.9	68.3	28.7	65.3	45.1	64.6	58.0	71.2	20.0	27.5	54.9	54.9	69.4	63.5
	MIST(+Reg) [22]	54.9	68.8	77.7	57.0	27.7	28.9	69.1	74.5	67.0	32.1	73.2	48.1	45.2	54.4	73.7	35.0	29.3	64.1	53.8	65.3	65.2
	CASD [14]	57.0	67.2	71.5	57.8	41.5	23.4	72.9	70.3	75.5	21.5	64.8	53.8	71.8	65.0	72.5	32.6	25.0	56.6	58.5	69.5	68.2
	CASD ²	57.4	56.1	64.6	61.4	60.9	35.1	59.9	76.9	56.6	27.8	73.6	51.2	60.1	70.5	72.5	34.4	54.0	70.5	45.1	53.1	63.7
CASD+W2N [13]	65.4	74.0	81.7	71.2	48.9	51.0	78.6	82.3	83.5	29.1	76.9	51.5	82.1	76.9	79.1	28.5	34.3	65.0	64.2	75.2	74.8	
Ours	D ² F2WOD _{casd}	64.8	62.7	64.9	69.9	47.9	57.9	74.3	85.7	59.6	43.4	82.2	39.6	67.2	84.0	77.8	74.0	50.6	74.6	48.8	66.7	64.6
	D ² F2WOD _{casd+w2n}	66.9	58.6	69.1	77.9	49.3	78.1	73.2	89.0	64.9	39.6	83.5	33.0	77.7	95.2	77.0	75.9	50.7	74.4	44.8	66.6	61.0
(b) SyntheticPizza10 \rightarrow RealPizza10.																						
Type	Method	mAP	Pepperoni	Mushroom	Pepper	Olive	Basil	Bacon	Broccoli	Pineapple	Tomato	Onion										
CD	Faster R-CNN [21]	4.3	12.1	0.4	9.6	5.0	3.4	0.3	1.0	1.0	9.7	0.9										
	DT+PL [15]	14.9	30.7	4.3	11.6	25.3	42.7	1.3	3.6	2.4	21.4	5.2										
	PADOD [12]	8.1	19.5	0.2	3.4	11.8	30.2	0.2	1.1	0.5	13.3	0.8										
Ours	D ² F2WOD _{warm-up}	17.9	31.0	8.3	11.8	28.1	45.5	0.8	9.8	9.8	21.5	12.7										
SD	OICR [32]	4.7	0.2	1.3	4.5	0.1	0	8.8	19.4	11.0	1.0	0.8										
	CASD [14]	12.9	12.7	19.5	14.8	10.5	13.7	10.4	10.1	14.5	11.7	10.7										
Ours	D ² F2WOD _{casd}	25.1	43.9	35.1	14.9	27.3	41.8	9.2	12.5	8.5	28.4	29.2										

current transformer-based detectors rely on relatively large amounts of annotate data; therefore, we found that it was difficult to train Sparse DETR on Clipart1K with only 500 training images; by contrast, Sparse DETR worked reasonably well on SyntheticPizza10 with 14,802 training images. Accordingly, for the experiment on the Clipart1K \rightarrow VOC2007 datasets, we mainly focus on Faster R-CNN. We leave the investigation of Sparse DETR on Clipart1K \rightarrow VOC2007 as interesting future work, by either exploring additional synthetic data to increase the synthetic training dataset size or leveraging more data-efficient transformer-based detectors.

- **Identifying Object Detection Errors.** We use TIDE [3] to analyse the **classification**, **localization**, **both Cls and Loc**, **duplicate detection**, **background**, and **missed GT** errors in DT+PL, CASD, and our model. Each chart shows the relative percentage of each type of error. As shown in Fig. 7, D^2F2WOD effectively reduces the localization error compared with other two baselines. Here classification error indicates object localized correctly but misclassified; localization error indicates object classified correctly but mislocalized; both Cls and Loc error indicates object misclassified and mislocalized; duplicate detection error indicates object matched with a GT which

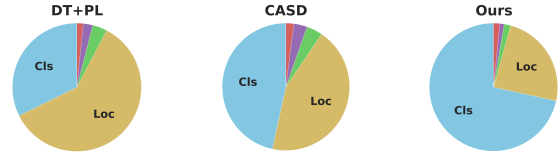


Figure 7: Summary of errors on DT+PL, CASD and our method.

has already matched with another higher confidence scoring prediction; background error indicates background detected as foreground; missed GT error indicates ground-truth that not matched with any predictions.

F. Additional Qualitative Analysis

Fig. 8 shows the representative images generated by CycleGAN on different benchmarks.

Fig. 9 illustrates some examples used for FSOD-3 training on SyntheticPizza10 \rightarrow RealPizza10.

Fig. 10 and Fig. 11 illustrate detection results produced by our D^2F2WOD and CASD on RealPizza10 and VOC2007 datasets, respectively. There, it can be observed that D^2F2WOD does not only locate most objects, but that it also produces more accurate bounding boxes. Specifically, in the RealPizza10 images it can be appreciated bounding

Table 9: Effectiveness of progressive adaptation: each adaptation step in our warm-up stage is helpful not only in terms of mAP, but also benefits for each class.

FSOD	Step	mAP	Pepperoni	Mushroom	Pepper	Olive	Basil	Bacon	Broccoli	Pineapple	Tomato	Onion
Faster R-CNN	FSOD-1	4.3	12.1	0.4	9.6	5.0	3.4	0.3	1.0	1.0	9.7	0.9
	FSOD-2	9.7	22.3	0.8	9.6	14.5	33.2	0.8	0.7	0.8	13.4	1.0
	FSOD-3	10.3	23.0	1.0	10.1	15.4	35.7	0.8	0.8	0.6	14.4	1.1
	FSOD-4	15.0	28.7	4.6	11.0	22.2	39.9	9.3	1.8	9.6	16.6	6.3
	FSOD-5	17.9	31.0	8.3	11.8	28.1	45.5	0.8	9.8	9.8	21.5	12.7
Sparse DETR	FSOD-1	3.7	10.0	0.2	0.8	20.2	0.7	0.2	0.4	0.6	1.0	2.6
	FSOD-2	9	27.0	1.7	0.6	24.5	19.1	0.1	2.3	2.5	8.3	4.0
	FSOD-3	10.3	30.40	0.9	1.2	28.1	27.7	0.0	1.2	1.3	9.2	2.5
	FSOD-4	18.2	47.7	4.7	5.9	39.8	46.0	0.0	1.7	3.1	25.1	7.8
	FSOD-5	18.5	48.3	6.0	5.3	43.0	43.1	0.1	1.4	2.4	26.1	9.2

Table 10: Impact of adaptation order (Faster R-CNN backbone).

Adaptation Domain	mAP	Pepperoni	Mushroom	Pepper	Olive	Basil	Bacon	Broccoli	Pineapple	Tomato	Onion
\mathcal{S}	4.3	12.1	0.4	9.6	5.0	3.4	0.3	1.0	1.0	9.7	0.9
$\mathcal{S} \rightarrow \mathcal{G}_1 \rightarrow \mathcal{G}_2$	10.3	23.0	1.0	10.1	15.4	35.7	0.8	0.8	0.6	14.4	1.1
$\mathcal{S} \rightarrow \mathcal{G}_2 \rightarrow \mathcal{G}_1$	5.9	5.8	1.1	9.7	6.9	20.4	0	2.3	0.5	9.1	3.2
$\mathcal{G}_2 \rightarrow \mathcal{T} \rightarrow \text{Aug.}\mathcal{T}$	17.9	31.0	8.3	11.8	28.1	45.5	0.8	9.8	9.8	21.5	12.7
$\mathcal{G}_2 \rightarrow \text{Aug.}\mathcal{T} \rightarrow \mathcal{T}$	17.3	32.6	6.3	8.3	28.4	47.3	0.6	4.9	10.4	22.4	11.3

Table 11: Generalizability of the warm-up stage across FSODs.

FSOD	Stage	mAP	Pepperoni	Mushroom	Pepper	Olive	Basil	Bacon	Broccoli	Pineapple	Tomato	Onion
Faster R-CNN	D ² F2WOD _{warm-up}	17.9	31.0	8.3	11.8	28.1	45.5	0.8	9.8	9.8	21.5	12.7
	D ² F2WOD _{casd}	25.1	43.9	35.1	14.9	27.3	41.8	9.2	12.5	8.5	28.4	29.2
Sparse DETR	D ² F2WOD _{warm-up}	18.5	48.3	6.0	5.3	43.0	43.1	0.1	1.4	2.4	26.1	9.2
	D ² F2WOD _{casd}	26.2	51.9	35.5	18.9	33.1	47.4	11.2	9.6	5.4	29.3	20.1

boxes provided by our method (left) closely align with the objects of interest, while for CASD (right) bounding boxes are often imprecise (either wrong shape or big/small). Similar observations can be made for VOC2007 where CASD often fails to locate objects or produces spurious bounding boxes.

Fig. 12 illustrates some challenging cases on the RealPizza10 dataset where the performance of both our D²F2WOD and the baseline CASD still lags. We hypothesize this is because in these cases, the corresponding categories (e.g., bacon, broccoli and pineapple) have significantly smaller number of training examples.

Table 12: Ablation study of D^2F2WOD main configurations on (a) Clipart1K \rightarrow VOC2007 (Faster R-CNN backbone), (b) SyntheticPizza10 \rightarrow RealPizza10 (Faster R-CNN backbone) and (c) SyntheticPizza10 \rightarrow RealPizza10 (Sparse DETR backbone). “FE” and “OP” denote the domain specific pre-trained feature extractor and weakly-supervised object proposal generator, respectively.

(a) Clipart1K \rightarrow VOC2007 (Faster R-CNN backbone).

Type	Method	mAP	aero	bike	bird	boat	bottle	bus	car	cat	chair	cow	table	dog	horse	mbike	person	plant	sheep	sofa	train	tv
SD	OICR	41.2	58.0	62.4	31.1	19.4	13.0	65.1	62.2	28.4	24.8	44.7	30.6	25.3	37.8	65.5	15.7	24.1	41.7	46.9	64.3	62.6
D^2F2WOD_{oicr}	+FE	44.7	53.8	52.5	41.1	37.4	27.8	53.9	63.5	39.1	30.5	59.5	40.7	42.6	47.6	52.1	23.5	36.1	55.9	40.0	45.1	50.7
	+OP	47.2	23.4	54.4	46.9	34.6	46.5	69.4	78.0	10.1	44.7	65.6	27.7	25.9	52.8	64.3	65.3	32.5	54.7	42.1	52.8	52.3
	+FE+OP	52.7	39.1	60.6	56.2	37.4	48.0	67.8	81.0	18.6	51.8	67.5	38.1	31.3	72.0	67.8	70.2	40.0	60.6	40.9	56.4	49.3
SD	CASD	57.0	67.2	71.5	57.8	41.5	23.4	72.9	70.3	75.5	21.5	64.8	53.8	71.8	65.0	72.5	32.6	25.0	56.6	58.5	69.5	68.2
D^2F2WOD_{casd}	+FE	60.0	51.0	71.1	72.1	38.1	27.5	76.1	71.6	74.0	27.2	64.3	58.8	81.6	88.1	71.0	63.1	19.5	53.2	58.7	69.4	64.0
	+OP	60.1	38.3	67.6	63.2	45.4	62.0	77.7	88.9	24.1	56.3	76.9	44.9	41.4	76.8	77.4	75.1	42.2	68.6	52.4	62.2	61.4
	+FE+OP	64.8	62.7	64.9	69.9	47.9	57.9	74.3	85.7	59.6	43.4	82.2	39.6	67.2	84.0	77.8	74.0	50.6	74.6	48.8	66.7	64.6

(b) SyntheticPizza10 \rightarrow RealPizza10 (Faster R-CNN backbone).

Type	Method	mAP	Pepperoni	Mushroom	Pepper	Olive	Basil	Bacon	Broccoli	Pineapple	Tomatoes	Onion
SD	OICR	4.7	0.2	1.3	4.5	0.1	0	8.8	19.4	11.0	1.0	0.8
D^2F2WOD_{oicr}	+FE	8.5	4.4	12.5	12.2	7.2	6.1	7.4	8.6	13.2	5.1	7.9
	+OP	12.6	23.0	18.5	8.5	14.7	20.8	5.0	2.3	3.9	13.9	15.8
	+FE+OP	13.8	24.3	19.7	10.0	15.2	21.9	3.7	7.5	3.6	16.3	15.4
SD	CASD	12.9	12.7	19.5	14.8	10.5	13.7	10.4	10.1	14.5	11.7	10.7
D^2F2WOD_{casd}	+FE	14.8	10.2	11.3	14.6	10.1	10.0	19.0	30.9	21.0	10.9	10.5
	+OP	24.0	45.8	36.7	14.8	25.8	37.4	3.2	12.3	3.5	32.1	28.3
	+FE+OP	25.1	43.9	35.1	15.0	27.3	41.8	9.2	12.5	8.5	28.4	29.2

(c) SyntheticPizza10 \rightarrow RealPizza10 (Sparse DETR backbone).

Type	Method	mAP	Pepperoni	Mushroom	Pepper	Olive	Basil	Bacon	Broccoli	Pineapple	Tomatoes	Onion
SD	OICR	5.9	12.1	9.9	2.8	5.4	12.7	1.0	0.3	0.1	5.5	9.4
D^2F2WOD_{oicr}	+FE	10.8	21.7	17.1	9.3	11.6	15.2	0.4	4.5	0.8	15.6	12.1
	+OP	13.4	22.1	16.8	9.0	13.5	23.7	10.9	5.5	2.2	15.6	14.3
	+FE+OP	15.4	28.0	13.2	9.5	21.5	24.1	8.0	14.0	7.7	19.6	8.3
SD	CASD	13.4	25.2	17.0	8.3	14.9	21.0	10.0	5.9	0.5	18.0	12.8
D^2F2WOD_{casd}	+FE	15.8	26.7	22.1	14.3	16.6	20.2	5.4	9.5	5.8	20.6	17.1
	+OP	25.1	44.5	35.0	14.6	28.7	46.2	8.6	8.5	3.8	31.7	29.1
	+FE+OP	26.2	51.9	35.5	18.9	33.1	47.4	11.2	9.6	5.4	29.3	20.1

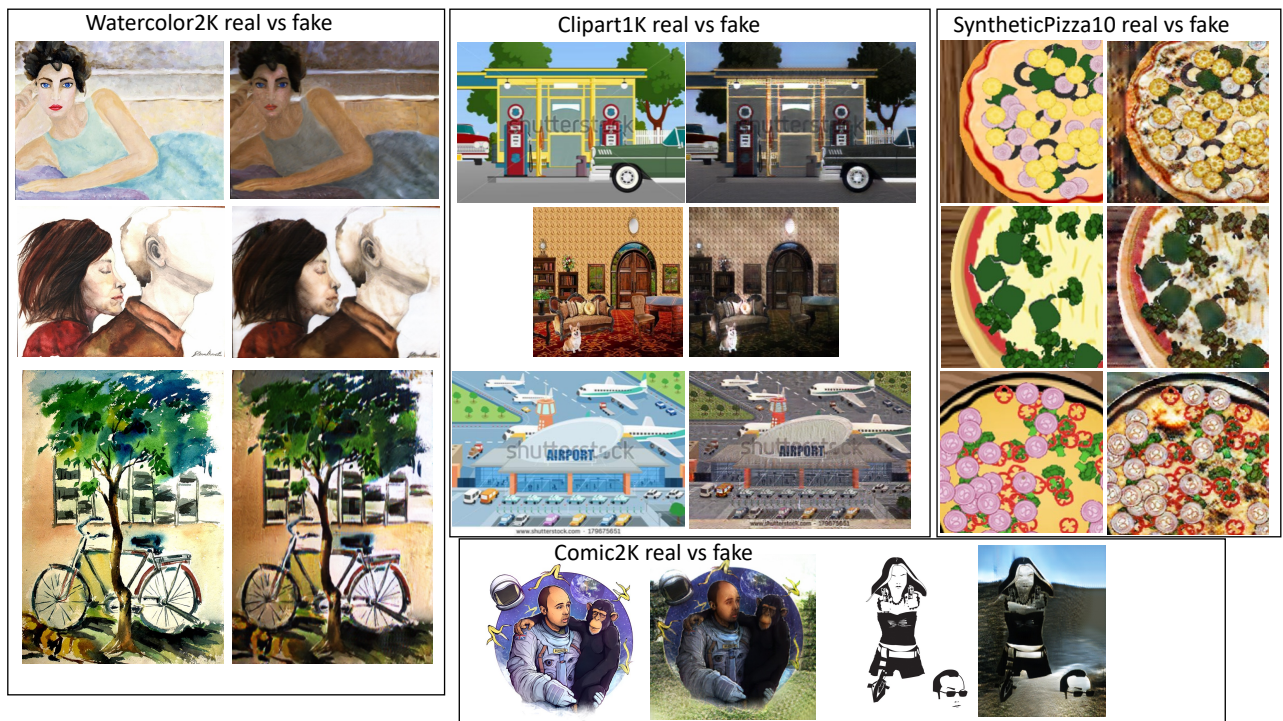


Figure 8: Representative images generated by CycleGAN.

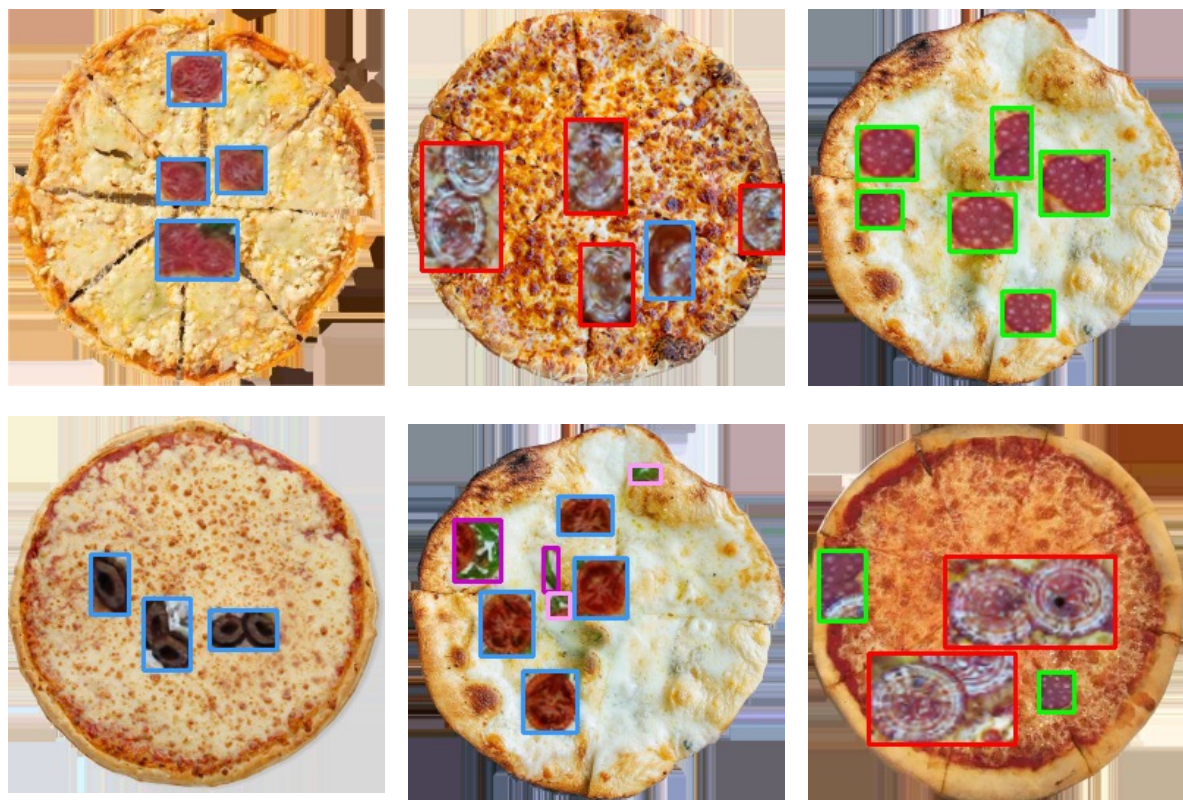


Figure 9: Representative images used for FSOD-3 training.

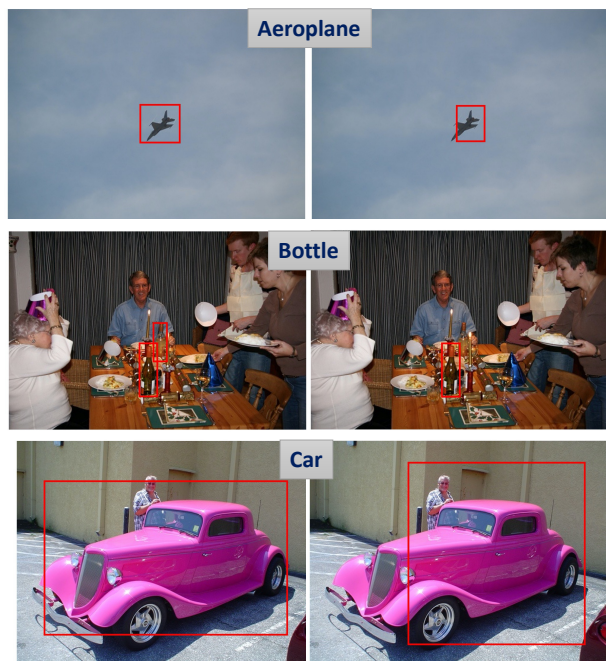


Ours vs. CASD

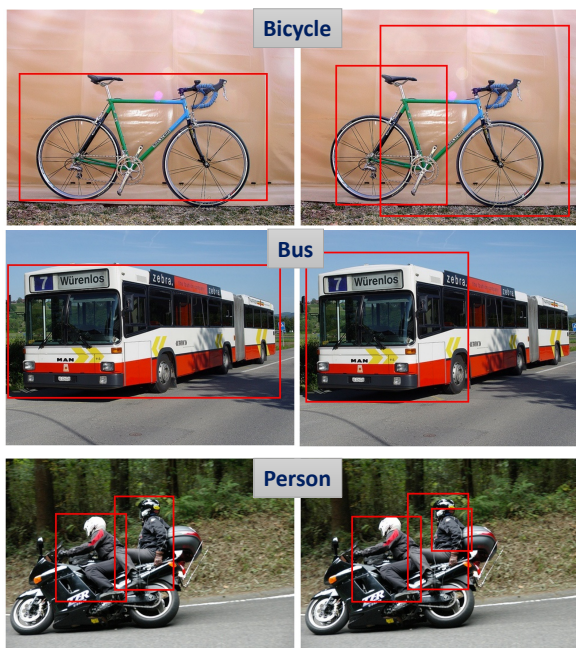


Ours vs. CASD

Figure 10: Example of success cases for our D^2F2WOD_{casd} vs. CASD in the test set of RealPizza10 dataset. We only show instances with scores over 0.3 to maintain visibility.



Ours vs. CASD



Ours vs. CASD

Figure 11: Example of success cases for our D^2F2WOD_{casd} vs. CASD in the test set of VOC2007 dataset. We only show instances with scores over 0.3 to maintain visibility.

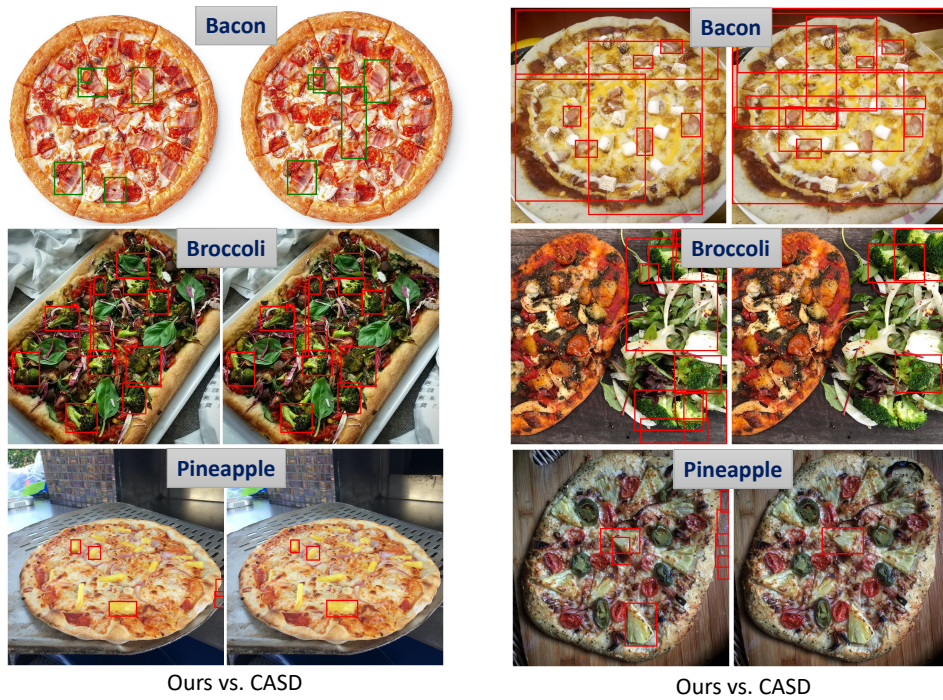


Figure 12: Challenging cases in the test set of Realpizza10 dataset where both our D^2F2WOD_{casd} and the baseline CASD fail. We hypothesize this is because these three categories have significantly smaller number of training examples. We only show instances with scores over 0.3 to maintain visibility.